Implementing plant hydraulics in the Community Land Model

Daniel Kennedy[1], **Sean Swenson**[2], **Keith Oleson**[2], **David Lawrence**[2], **Rosie Fisher**[2], **Pierre Gentine**[1]

[1]Columbia
[2]National Center for Atmospheric Research, Table Mesa Drive, Boulder, Colorado, USA

Key Points:

- A simplified soil-plant-atmosphere continuum model based on hydraulic theory is implemented in the Community Land Model (version 5).
- Prognostic leaf water potential replaces soil matric potential as the functional basis for water stress, thus reflecting how the leaf water supply (via the xylem network) and evaporative demand act in concert to determine plant water status and thus stomatal conductance and leaf gas exchange.
- Prognostic root water potential is used to implement hydraulic root water uptake, replacing the heuristic soil 'wilting' factor .

Corresponding author: Daniel Kennedy, djk2120@columbia.edu

Abstract

= enter abstract here =

1 Introduction

Trees face emerging climate change risk globally [*Allen et al.*, 2010; *Anderegg et al.*, 2013a]. Understanding vegetation response is a high priority, both for discerning climate impacts and for modeling feedbacks to the carbon and hydrological cycles. In addition to stress from soil moisture drought, vegetation is susceptible to increasing atmospheric transpiration demand [*Restaino et al.*, 2016; *Novick et al.*, 2016a]. Increases in vapor pressure deficit (VPD) have occurred with warming [*Ficklin and Novick*, 2017; *Seager et al.*, 2015], and are associated with impacts on vegetation [*Williams et al.*, 2013; *Mcdowell and Allen*, 2015]. Significant uncertainty remains regarding how vegetation will respond to changes in hydroclimate within Earth System Models, feeding back onto the carbon cycle as vegetation mediates carbon uptake [*De Kauwe et al.*, 2017; *Friedlingstein et al.*, 2014].

Plant water stress parameterizations are important in Earth System Models, as they define vegetation regulation of surface fluxes (photosynthesis, transpiration) to water fluctuations. Vegetation water use strategies also modulate carbon uptake, creating a critical coupling between the Earth System's carbon and hydrological cycles [*Green et al.*, 2017]. Drought stress parameterizations (functions which relate simple metric of soil moisture status to leaf gas exchange) are widely used to define the response of stomatal conductance to vegetation water status that is used to attenuate transpiration, photosynthesis, and root water uptake with drying. The dynamics of water stress in models have broad effects on critical land surface processes [*Joetzjer et al.*, 2014]. On diurnal timescales, water stress parameterizations influence the partitioning of latent versus sensible heat with effects on surface temperature [*Bonan et al.*, 2014]. On longer timescales vegetation water use strategies regulate the global carbon and water cycles [*De Kauwe et al.*, 2015].

Many recent studies have aimed at advancing the representation of water flow through the Soil-Plant-Atmosphere continuum (SPAC) in land models [*Xu et al.*, 2016; *Christoffersen et al.*, 2016; *Sperry et al.*, 2017]. Explicit modeling of water flow through the SPAC adds complexity, but is consistent with evidence of dynamic regulation of vegetation water use in response to both soil and atmospheric drying [*Sperry and Love*, 2015]. Furthermore, via Darcy's Law, SPAC models have a robust physical basis. SPAC models involve new parameters, which presents new challenges [*Drake et al.*, 2017], but plant hydraulic trait information is available [*Kattge et al.*, 2011; *Anderegg*, 2015a], providing guidance on parameter estimation. and can be informative of forest vulnerability to drought [*Choat et al.*, 2012]. Likewise vegetation water status observations are available at a scale that is directly relevant to model development [*Konings et al.*, 2016; *Grant et al.*, 2016] and can be used to validate model results [*Momen et al.*, 2017; *Konings et al.*, 2017b].

The empirical representation of vegetation water stress in the Community Land Model (CLM) and other land surface models is a known deficiency, with implications for the representation of the dry/wet season in tropical rainforests [*Powell et al.*, 2013; *Ukkola et al.*, 2016].

In this study, we develop a plant hydraulic implementation within the recently released CLM version 5 (CLM5), based on hydraulic theory, which we refer to as the 'Plant Hydraulic Stress' (PHS) configuration. We analyse the dynamics of the new PHS model using site-level simulations that replicate the Caxiuanã, Brazil through-fall exclusion experiment [*Fisher et al.*, 2006].

Advancing the representation of the SPAC introduces the representation of vegetation water potential (discretized into leaf, stem and root elements) into the CLM, as well as an explicit representation of water supply, from the soil through the vegetation substrate. Tran-

spiration is attenuated with drought stress according to vegetation water status, capturing dynamic vegetation water use regulation. These changes have numerous implications, including

1. Leaf water potential serves as an improved metric for water status (compared to soil water or soil matric potential), since it reflects vegetation sensitivity to both soil and atmospheric drying, while serving as a diagnostic for excessive xylem tension and cavitation risk.

2. Modeling and plant hydrodynamics provides a framework for representing hydraulic redistribution [*Lee et al.*, 2005]

3. Modeling vegetation water potential allows improved connection to remote sensing observations (e.g. Vegetation Optical Depth) [*Konings et al.*, 2016].

4. Further, root water potential can be used to predict gradient-based root water uptake based on Darcy's law, replacing the previous empirical transpiration partitioning heuristic. This provides the means to vary, for example, the mean depth of extraction with changing soil water conditions.

5. The new model can represent a range of water use strategies, improving the connection between plant carbon allocation decisions and water availability.

SAY IN WHICH SECTION WE WILL FINE EACH PART

To assess the new model formulation, we carried out site-level simulations at Caxiuanã National Forest in Brazil, which features a critical biome (terra-firme moist tropical evergreen forest). Starting in 2001, a plot at this site was subjected to an approximately 50% percent precipitation through-fall exclusion. Due to the large drop in soil moisture at the precipitation exclusion site, we expect and observe [*Fisher et al.*, 2007] significant vegetation regulation of transpiration and photosynthesis.

In this paper we 1. Introduce the PHS theory and implemention in the CLM 2. Analyze the dynamics of modeled water stress, root water uptake and soil moisture profiles. 3. Compare PHS to the behaviour of the default CLM water stress configuration. 4. Discuss the benefits and limitations of the new model.

2 Model Description

2.1 Photosynthesis

The CLM5 photosynthesis model is described in *Bonan et al.* [2011], *Thornton and Zimmermann* [2007], and *Oleson et al.* [2013].Photosynthesis is defined in three regimes: Rubisco-limited, light-limited, and export-limited following *Farquhar et al.* [1980] and *Harley et al.* [1992].The implementation extends *Sellers et al.* [1996a,b] with co-limitation following *Collatz et al.* [1991].

CLM5 photosynthesis, in its default configuration, is a two-big-leaf model, with a sunlit and shaded leaf for each plant functional type [*Thornton and Zimmermann*, 2007; *Dai et al.*, 2004; *Oleson et al.*, 2013]. The canopy fluxes module iterates the solution for leaf temperature to satisfy the leaf surface energy balance, while environmental conditions are evolving. Within this, the photosynthesis module further iterates to solve for inter-cellular CO_2 concentration, balancing stomatal flux of CO_2 with photosynthetic assimilation flux of CO_2.

2.2 Stomatal Conductance

CLM5 implements the Medlyn stomatal conductance model, which reconciles the empirical and optimal approaches to modeling stomatal conductance [*Medlyn et al.*, 2011]. Stomatal conductance of CO_2 is thus directly related to net photosynthesis (A_n), CO_2 concentration at the leaf surface (C_a), and the square root of the vapor pressure deficit near the

leaf surface ($\sqrt{D}$).

$$g_s = g_0 + \left(1 + \frac{g_1}{\sqrt{D}}\right)\frac{A}{C_a} \tag{1}$$

The model features two parameters g_0 (μmol / m2 / s) and g_1 (kPa$^{0.5}$). The g_0 parameter is minimum stomatal conductance, representing cuticular and epidermal losses (small). The g_1 parameter relates to the marginal water cost guiding the optimization of carbon assimilation. These parameters are plant functional type dependent.

The Medlyn model, derived from stomatal optimization theory, predicts stomatal conductance to maximize assimilation relative to water costs ($A - \lambda E$), but does not resolve concurrent limitations to stomatal conductance associated with drought conditions. These water stress factors (in our case, f_w), are used to represent stomatal and non-stomatal limitation not captured by the leaf-level stomatal conductance model (which can be thought of as a prediction of maximum stomatal conductance in these cases). To represent soil drought, and its impact on diffusive fluxes, land surface models typically include a 'water stress factor'(f_w, dimensionless, 0 to 1, formerly β_t). Uncertainty remains within the literature for how to apply water stress factors to photosynthesis and/or stomatal conductance. [*Zhou et al.*, 2013; *Novick et al.*, 2016b; *Sperry and Love*, 2015].

In CLM, f_w multiplies the rate of maximum carboxylation (V_{cmax}) as described in *Oleson et al.* [2013]. Other models opt for soil-moisture based stomatal limitation (linking the stomatal conductance model slope parameter to soil moisture), however, *Lin et al.* [2018] found that only g_0 was sensitive to soil moisture (and not g_1). *Zhou et al.* [2013] suggest that changes in assimilation tend to exceed those predicted by modulating g_1 with soil moisture, but could be captured by changing V_{cmax}. Other field studies, however, suggest that V_{cmax} does not change with drought, whereby modeled V_{cmax} instead may implicitly account for mesophyll conductance changes [*Flexas et al.*, 2004].

In PHS, we opt for a simplified form of this stress approach, which seems to be consistent with field observations [*Lin et al.*, 2018]. Prognostic water stress (f_w, ranging from 0-1) attenuates stomatal conductance indirectly via multiplication of V_{cmax}. Water stress then lowers assimilation, which is coupled to stomatal conductance ([*Medlyn et al.*, 2011]).

f_w is modeled here as a function of leaf water potential (ψ_{leaf}) (see Section 2.3.3), with stress increasing as ψ_{leaf} becomes more negative. This reflects the concept of hydraulic safety, with vegetation avoiding excessive xylem tension associated with risk of cavitation.

Utilizing leaf water potential adopts a framework where stomatal conductance optimized for carbon gain is concurrently limited by hydraulic constraints [*Novick et al.*, 2016b]. As a result, low soil water (bottom-up stress) can induce leaf moisture stress due to limited water supply while high atmospheric VPD can also induce leaf moisture stress by propagating a drying into the xylem (top-down stress).

Much recent work has focused on alternative constraints on plant hydrodynamics, especially in response to drying soils [*Manzoni et al.*, 2013a; *Novick et al.*, 2016b; *Zhou et al.*, 2014]. This includes how plants manage the risk of cavitation associated with increasing xylem tension [*Sperry et al.*, 1998]. [*Sperry et al.*, 2017], for example, argue that theory based on hydraulic costs (define) could be used instead of optimizing of $A - \lambda E$. Otherwise, the marginal water cost might be adjusted based on soil water status by adjusting λ or Medlyn g_1 [*Manzoni et al.*, 2013a], but this may underestimate drought effects on photosynthesis *expand on this-RF*[*Zhou et al.*, 2013; *Lin et al.*, 2018]. A hybrid approach, combines stomatal optimization with hydraulic constraints and/or so-called non-stomatal limitation, where stress attenuates V_{cmax} or mesophyll conductance (both of which feed back through photosynthesis to lower stomatal conductance) [*Egea et al.*, 2011; *Novick et al.*, 2016b]. [*link this back to which options are used in PHS -RF*]

2.3 Plant Hydraulic Stress (PHS)

The PHS model within CLM5 uses hydraulic (Darcy's) law and a corresponding electrical circuit analogy (Figure 1), to model the flow of water through the SPAC. The hydraulic framework is used to diagnose water stress associated with increasing xylem tension and to calculate the root water uptake in each of (in this case) 20 vertically discretized soil layers.

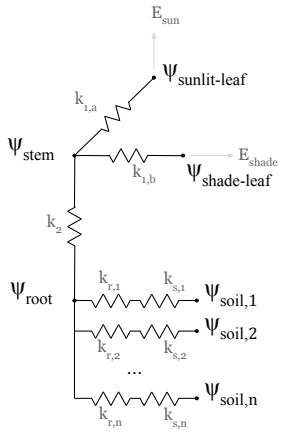

Figure 1. Plant hydraulic circuit analog schematic

2.3.1 Hydraulic schematic and segmentation

PHS solves for the set of SPAC vegetation water potential values (ψ_{root}, ψ_{stem}, $\psi_{\text{shade-leaf}}$, $\psi_{\text{sun-leaf}}$) that matches water supply (root water uptake) to water demand (transpiration), while maintaining continuity of water flow throughout the SPAC. Segmentation and other model design decisions followed a preference for a simplified implementation that whenever possible conformed to existing CLM model structure.

At each node in the circuit diagram in Figure 1 we model water potential, and, between nodes, we resolve the flux of water. The choice of nodes for segmentation is designed to take advantage of field-measured hydraulic traits and to allow for differences in segment parameterizations [*Simonin et al.*, 2015; *Sperry and Love*, 2015]. As in other versions of the CLM, PHS uses vertically discretized soil layers and a two-layer (sunlit vs. shaded) canopy. Water uptake from the different soil layers is assumed to operate in parallel; a typical assumption justified by higher resistance in lateral versus central roots (e.g. Williams et al. 2001). We further separate resistance through the soil matrix from the resistance through the root tissue [*Williams et al.*, 1996]. Specifics on the parameterization of conductance for each segment are provided in Appendix B.1.

2.3.2 Water supply

Water supply is modeled via Darcy's Law, where flow of water (q) is the product of the path hydraulic conductance (k) and the gradient in water potential (accounting for changes in gravitational potential). Equation 2 represents the flow from a generic node 1 to node 2.

$$q = -k\left(\psi_2 - \psi_1 - \rho g \Delta z\right) \tag{2}$$

PHS does not represent plant tissue water storage (or capacitance, using the electrical circuit analogy). Capacitance significantly complicates the water potential solution [*Celia et al.*, 1990] and is challenging to parameterize [*Bartlett et al.*, 2016]. However, buffering

of water stress provided by tissue water storage could potentially be important especially on sub-daily timescales [*Meinzer et al.*, 2009; *Epila et al.*, 2017], whereby its inclusion may be warranted in future model generations.

Vegetation segment conductance is modeled following empirical xylem vulnerability curves [*Tyree and Sperry*, 1989], where segments lose conductance with increasing xylem tension related to cavitation and embolism [*Holbrook et al.*, 2001]. The vulnerability curves model loss of conductance relative to maximum conductance using two parameters: c_k, a sigmoidal shape-fitting parameter, and p_{50}, the water potential at 50% loss of segment conductance (following *Gentine et al.* [2016]).

Both c_k and p_{50} can be estimated from field experiments [*Sack et al.*, 2002], and p_{50} is available in the TRY trait database [*Kattge et al.*, 2011]. Parameterization based on p_{50} aligns with the call for a transition to models that use a wider range of plant functional trait data in their parameterization [*Anderegg*, 2015a]. The loss of xylem conductivity is based on lower terminal water potential (ψ_1) as is typical in other simplified models [*Xu et al.*, 2016], but may underestimate the integrated loss of conductivity [*Sperry and Love*, 2015].

$$k = k_{\max} 2^{-\left(\frac{\psi_1}{p_{50}}\right)^{c_k}} \tag{3}$$

PHS models root, stem, and leaf tissue conductances according to equation 3. The parameterization of $k_{\max}$ varies by hydraulic segment (see details in Appendix B1). The conductance across the soil matrix to the root surface follows *Williams et al.* [2001] and *Bonan et al.* [2014] and estimates a characteristic distance between the bulk soil and the root surface, to facilitate length-scaling of soil conductivity. Bulk soil resistivity is based on *Clapp and Hornberger* [1978] as described in *Oleson et al.* [2013]. Further details are provided in Appendix B1.

2.3.3 Water demand

Vegetation water demand and stomatal regulation is based on the Medlyn stomatal conductance model (see Section 2.2), which we adjust using the water stress factor f_w. As discussed earlier, f_w is based on leaf water potential [*Klein and Niu*, 2014], and multiplies V_{cmax}, thus attenuating photosynthesis, and thus also stomatal conductance and transpiration.

As leaf water potential declines (because of transpiration) and xylem tension increases, transpiration is attenuated relative to its maximal value. The maximum transpiration ($E_{\text{sun,max}}$, $E_{\text{shade,max}}$) is defined as the value that results from Medlyn stomatal conductance in the absence of water stress (achieved by setting $f_w = 1$). The fraction of maximum transpiration is modeled with a two-parameter sigmoidal function (Equation 4).

$$\begin{aligned} E_{\text{sun}} &= E_{\text{sun,max}} 2^{-\left(\frac{\psi_{\text{sun-leaf}}}{\psi_{50}}\right)^{c_k}} \\ E_{\text{shade}} &= E_{\text{shade,max}} 2^{-\left(\frac{\psi_{\text{shade-leaf}}}{\psi_{50}}\right)^{c_k}} \end{aligned} \tag{4}$$

Where ψ_{50}, is the leaf water potential at 50% loss of transpiration and c_k is a sigmoidal shape-fitting parameter.

We define f_w as the ratio of attenuated to maximal stomatal conductance (Equation 5). Maximum stomatal conductance ($g_{\text{s,sun,max}}$, $g_{\text{s,shade,max}}$) is computed as the stomatal conductance in the absence of water stress, i.e. $f_w = 1$. The attenuated stomatal conductance ($g_{\text{s,sun}}$, $g_{\text{s,shade}}$) is then the stomatal conductance associated with the PHS module water flow solution, which matches vegetation water supply with vegetation water demand (Section 2.3.4).

$$f_{\text{w,sun}} = \frac{g_{\text{s,sun}}}{g_{\text{s,sun,max}}}$$
$$f_{\text{w,shade}} = \frac{g_{\text{s,shade}}}{g_{\text{s,shade,max}}} \tag{5}$$

Whereas the water supply parameters (see Section 2.3.2) relate to hydraulic traits often measured in the field, the hydraulic demand parameters ψ_{50} and c_k reflect the emergent property of hydraulic limitations to transpiration and must be empirically derived (WHAT ABOUT PLC CURVES?).

CLM also features two empirical stomatal control parameters, which are the soil matric potentials where stomata are either fully closed (θ_{wilt}) or fully open (θ_{crit}) (see Section 3). Recent modeling studies have proposed different forms of relationship between stomatal regulation with water stress [*Sperry et al.*, 2017; *Xu et al.*, 2016; *Christoffersen et al.*, 2016] and thus this representation remains the topic of active research .

2.3.4 PHS solution

PHS solves for the set of vegetation water potential values (ψ) that matches water supply (root water uptake) to water demand (transpiration), while satisfying continuity across the four water flow segments (soil-to-root, root-to-stem, stem-to-leaf, and leaves-to-transpiration). At each time step, PHS computes the flux divergence f (representing the mismatch of flow in and out of each segment for a given set of vegetation water potential values ψ_i, and iteratively updates ψ until convergence is reached in terms of divergence, $f \to 0$.

$$\psi = \begin{bmatrix} \psi_{\text{sun}} \\ \psi_{\text{shade}} \\ \psi_{\text{stem}} \\ \psi_{\text{root}} \end{bmatrix} \tag{6}$$

$$f(\psi) = \begin{bmatrix} E_{sun} - q_{sun} \\ E_{shade} - q_{shade} \\ q_{sun} + q_{shade} - q_{stem} \\ q_{stem} - \sum_{j=1}^{n} q_{root,j} \end{bmatrix} \tag{7}$$

$$A = \frac{df}{d\psi} \tag{8}$$

While $|f| > 0$

$$\Delta\psi = A^{-1} f(\psi_i)$$
$$\psi_{i+1} = \psi_i + \Delta\psi \tag{9}$$

The numerics are tractable because f has analytical derivatives and A (a 4x4 matrix with six null entries) is easy to invert when well-conditioned. Supply and demand converge, because transpiration demand decreases with more negative leaf water potentials and supply increases with more negative leaf water potentials. Within a set of PHS iterations (9), transpiration is assumed to be linear with f_w.

The PHS loop is nested within iterations for intercellular CO_2 concentration and leaf temperature. The non-linear relationship between f_w and transpiration is resolved through iteration for converging f_w alongside intercellular CO_2. Details on the numerical implementation are provided in Appendix Section B.1.

3 Water stress factor, SMS vs. PHS

PHS alters the transpiration beta function (β_t, colloquially BTRAN ,Equation 10), SAY WAHT IT IS which is the phenomenological soil water stress function in used in prior versions of CLM, as described in *Oleson et al.* [2013]. Because the name β_t is associated with this specific plant hydrodynamics representation, we opt to rename the variable to the water stress factor f_w. Throughout this paper we refer to the original CLM plant hydrodynamics framework as SMS (soil moisture stress), as compared to the newer implementation described here, PHS (plant hydraulic stress). We adopt this terminology (in lieu of CLM4.5 vs. CLM5), because SMS is still deployable with CLM5. In this section we present the SMS version of f_w and outline the differences as compared to PHS

With PHS, we interpret f_w as a drought safety mechanism, attenuating stomatal conductance to avoid excessive xylem tension associated with very negative leaf water potential. As such, f_w is parameterized as a function of prognostic leaf water potential. With SMS, f_w is calculated based on soil matric potential, as a root-fraction weighted average potential departure from an empirical soil layer wilting factor (Equation 10). Recent studies suggest that the SMS parameterization introduces model bias in turbulent fluxes [*Bonan et al.*, 2014] and contributes to unrealistic drought response of photosynthesis and stomatal conductance [*Powell et al.*, 2013].

In SMS, the variable f_w is unitless, ranging from 0 to 1, with 1 corresponding to no water stress, and 0 corresponding to fully water stressed. It is calculated based on a root-fraction weighted average of soil layer wilting factor (w_i), which is a bounded linear function of soil water potential (ψ_i) relative to PFT parameters defining the soil potential with stomates fully open (ψ_o) and fully closed (ψ_c), among the soil layers $i = 1, \ldots, n$. Note that root fraction (r_i) sums to 1, by definition.

$$f_w = \sum_{i=1}^{n} r_i w_i \tag{10}$$

$$w_i = 0 \leq \frac{\psi_i - \psi_c}{\psi_o - \psi_c} \leq 1 \tag{11}$$

3.1 Root water uptake in SMS vs. PHS

Such parameterizations (WHICH ONES?) have primarily been examined with application to stomatal conductance, but they are also used to define vegetation soil water extraction. Each timestep, the transpiration flux solution must be distributed among the vertically discretized soil layers. In the SMS framework, the transpiration sink is partitioned by layer according to the soil layer wilting factor and root fraction.

In both stress parameterizations, f_w multiplies V_{cmax} to attenuate photosynthesis and stomatal conductance with soil water stress. With SMS, it is also directly used for modeling vegetation water extraction from the soil column. The total transpiration (T) is partitioned among the soil layers based on the f_w wilting factor. Within each soil layer, the contribution to total transpiration (q_i) depends on the layer root fraction and wilting factor, normalized by f_w:

$$q_i = \frac{r_i w_i}{f_w} T \tag{12}$$

Contrary to the heuristic SMS parameterization, the PHS implementation adopts a physically-based hydraulic framework, where the root water uptake (q_i) is the product of the hydraulic conductance (k_i) and the gradient in water potential (-$\Delta\psi$) driving the flow, i.e. obeying Darcy's law. That gradient is the difference between the root water potential (ψ_{root})

and the layer soil water potential (ψ_i), minus changes in gravitational potential, following Darcy's law.

$$\begin{aligned} q_i &= -k_i \Delta\psi \\ \Delta\psi &= (\psi_{\text{root}} - \psi_i - \rho g \Delta z) \end{aligned} \tag{13}$$

For comparison between SMS and PHS, we recast (12) into the hydraulic framework: defining $T_{\max}$, such that: $T = f_w T_{\max}$ to replace T in (12), and replacing w_i in (12) with the formula from (11).

$$q_i = \frac{T_{\max}}{\psi_o - \psi_c} r_i \left(\psi_i - \psi_c\right) \tag{14}$$

This yields SMS analogs for the hydraulic conductance and gradient terms of Equation 13.

$$\begin{aligned} k_i &= r_i \frac{T_{max}}{\psi_o - \psi_c} \\ \Delta\psi &= \psi_c - \psi_i \\ \text{constrained by:} \qquad \Delta\psi &= \begin{cases} 0 & \text{if } \psi_i < \psi_c \\ \psi_c - \psi_o & \text{if } \psi_i > \psi_o \end{cases} \end{aligned} \tag{15}$$

We use this formulation to discuss some of the implications for root water uptake from the former SMS parameterization of water stress (Equation 15).

3.2 Constant pulling potential

With SMS, that gradient is defined for each soil layer as the difference between the soil water potential in that layer (ψ_i) and a constant parameter, the soil water potential when stomata are fully closed (ψ_c). This parameter serves as the vegetation "pulling" potential for calculating the soil transpiration sink.

Using a constant wilting point is inconsistent with extensive evidence from the field of dynamic vegetation water potential, and cohesion tension theory (CITATIONS NEEDED) driving the transpiration flow. Likewise the values for ψ_c are quite negative, (-2.5 MPa for broadleaf evergreen tropical, BET, forests). *Fisher et al.* [2006] measured midday stem potential consistently higher than -0.5 MPa during the wet season, and on average -1.69 and -1.53 MPa during the dry season in the control and exclusion plots, respectively.

3.3 Conductance dynamics

In SMS, in lieu of dynamic vegetation water potential, intra-day SMS soil sink dynamics derive from a highly variable conductance (CLARIFY). As inferred in Equation 15, SMS conductance is modeled as a function of T_{max}, and three constant parameters. T_{max} is highly dynamic, responding to the diurnal course in transpiration demand. This is inconsistent with general principles of porous media flow, where conductivity is a function of the hydraulic architecture and its wetted status. Likewise, this representation of conductance does not represent the characteristic phenomenon where vessels lose conductance with drying.

3.4 No dependence on belowground carbon allocation

As is typical in water stress parameterizations, the SMS conductance is scaled by layer using an area basis, here using the relative vertical root fraction is used. With PHS, an absolute measure of root biomass is used (see Appendix Equation B.7), so that the belowground water cycle interacts with carbon allocation to the roots. An absolute measure better conforms with the physics of porous media flow and better responds to varying carbon allocation

strategies. For example, with SMS, if root mass doubles in every soil layer, the root access to water remains unchanged.

3.5 Lacks penalties for extraction from depth

Both PHS and SMS account for the effect of decreasing root area with depth (PHS, root area; SMS, root fraction), but PHS implements two other penalties for extracting water from deep in the soil column that are missing from SMS. The first is minor, but water extracted from depth must overcome gravity, amounting to about 0.01 MPa per meter in depth. This is missing from SMS and included with PHS. Likewise, SMS ignores the fact that hydraulic conductance is generally taken to scale with the inverse of conducting length. Deeper roots feature longer root tissue conducting length, and root spacing within the soil is less dense, requiring longer conducting distances across the soil matrix.In PHS, both these processes result in diminished hydraulic conductance (UNCLEAR).

3.6 Constraints

With SMS, the gradient in water potential is constrained between 0 and the range of soil potential between parameters for stomata fully open and closed (Equation 15). The upper constraint caps the gradient in water potential when soil potential reaches the value for stomata fully open (ψ_o=-0.65 MPa for BET). Darcy's Law predicts that the gradient in water potential would continue to increase until saturation matric potential. The lower constraint caps the gradient in water potential at zero, disallowing negative gradients. However, reversed water fluxes, caused by positive gradients in water potential from root to soil, have been observed in the field [*Burgess et al.*, 1998]. Both constraints are eschewed with PHS.

4 Experiment Description

All four simulations in this paper use the same development version of CLM5 (development version r270, https://github.com/ESCOMP/ctsm/releases/tag/clm4_5_18_r270).

The four simulations are used to assess the impact of the plant hydrodynamics model (PHS vs. SMS) on a through-fall experiment (i.e., with either ambient or 60% through-fall excluded), with all other model components and forcing shared. Simulations are run offline (uncoupled from an active atmospheric model), spanning from 2001 through 2003, utilizing the satellite phenology (SP) mode of CLM5 in which vegetation state (LAI, canopy height) is prescribed and biogeochemistry is inactive. All simulations start from the same initial conditions, which are obtained from a 9-year spin-up that repeats the PHS/Ambient simulation three times. To avoid duplication, descriptions of site characteristics, forcing data, and observational sap flux, can be found in *Fisher et al.* [2007].

4.1 Parameter Values and Through-fall Exclusion

Selected parameter values concerning vegetation hydrodynamics are presented in Table 1. All other parameters use the default values associated with the r270 version of CLM5. Informed by *Fisher et al.* [2008], we tuned soil hydraulic parameters and through-fall exclusion rates to reasonably capture the observed soil water dynamics (*Fisher et al.* [2007] Figure 4), Supplementary Figure **??**. Likewise, we tuned k_{max} and g_1 parameters to improve the fit to sap flux observations in the ambient simulation. The object of this paper is to present the dynamical impact of PHS to clearly describe model functionality. Model skill and parameter sensitivity will be assessed in follow-up studies.

371 **Table 1.** Select parameter values

CLM name	Full Name	Symbol	Value
kmax(1)	Maximum Sun Branch Conductance	$k_{1a,\max}$	4e-8 s^{-1}
kmax(2)	Maximum Shade Branch Conductance	$k_{1b,\max}$	4e-8 s^{-1}
kmax(3)	Maximum Stem Conductivity	$k_{2,\max}$	4e-8 m/s
krmax	Maximum Root Conductivity	$k_{r,\max}$	6e-9 m/s
psi50	Water potential at 50% loss of conductivity	ψ_{50}	-1.75 MPa
ck	Vulnerability shape parameter	c_k	2.95
smpso	Soil potential with stomata fully open	ψ_o	-0.65 MPa
smpsc	Soil potential with stomata fully closed	ψ_c	-2.5 MPa
medlyn_intercept	Medlyn intercept	g_0	100 μmol / m2 / s
medlyn_slope	Medlyn slope	g_1	6 $kPa^{0.5}$
n	Soil porosity to 4.64 meters	n	0.42
n	Soil porosity beyond 4.64 meters	n	0.28
hksat	Saturated soil hydraulic conductivity	$k_{\mathrm{s,max}}$	3e-5 m/s
sucsat	Saturated soil matric potential	ψ_{sat}	461 Pa
bsw	Brooks-Corey parameter	b	6

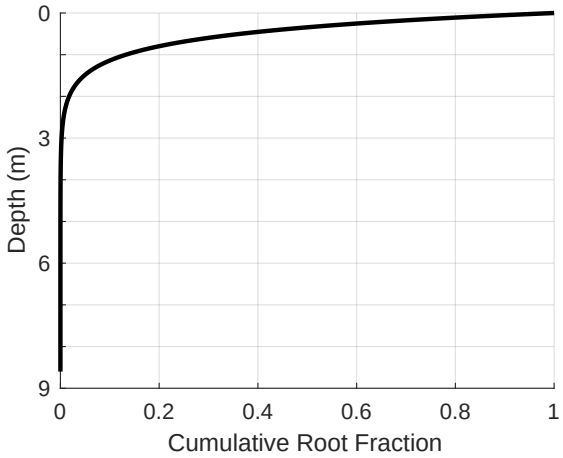

380 **Figure 2.** Cumulative rooting distribution

381 ## 5 Results

382 ### 5.1 Vegetation water potential

383 PHS introduces prognostic vegetation water potential to CLM at four locations within
384 the plant structure: at the root, stem, shaded leaf, and sunlit leaf. Under ambient conditions,
385 2003 dry season (September-October-November) model average sunlit leaf water potential
386 is -1.65 MPa at midday (local time 12-14h, Figure 3a). The midday pressure drop is primar-
387 ily between ψ_{root} and ψ_{stem}, representing the root collar and upper stem, respectively. Un-
388 der TFE, model midday leaf water potential decreases to -2.31 MPa (Figure 3b). Partitioned
389 among the segments of the SPAC, the change in leaf water potential (totaling -0.66MPa) due
390 to TFE is: -0.44MPa soil potential, -0.66MPa soil-to-root, +0.45MPa root-to-stem, and -
391 0.001MPa stem-to-leaf. This comports with previous evidence that seasonal changes in hy-
392 draulic resistance are larger belowground [*Fisher et al.*, 2006].

393 Modeled root water potential values match wet season observations, but are less nega-
394 tive than dry season observations under ambient conditions [*Fisher et al.*, 2006]. Midday leaf

411 **Table 2.** Root-zone soil potential [a] (MPa) terciles for Figure 5

Simulation	T1	T2
SMS, Ambient	-0.01	-0.54
SMS, TFE	-0.29	-1.74
PHS, Ambient	-0.01	-0.05
PHS, TFE	-0.05	-0.33

[a] SMS values correspond to daily mean root-fraction weighted soil potential. PHS values correspond to predawn root water potential.

395 water potential features a seasonal cycle, with lower values during the dry season (Figure 3c).
396 Modeled leaf water potential values under ambient conditions are less negative than averages
397 reported by *Fisher et al.* [2006] (1.71 MPa during the wet season and -2.47 MPa during the
398 dry season), but are within the range of observations. The model seems to underestimate iso-
399 hydricity in response to TFE, showing a drop in leaf water potential of 0.66MPa (dry season,
400 2003), whereas observations showed no significant difference.

401 ### 5.2 Stress factor

402 Average midday stress values are comparable during the 2003 dry season (Figure 4)
403 with the two model configurations. Under ambient conditions, the average stress factor val-
404 ues are 0.59 and 0.54 for SMS and PHS, respectively (dry season, midday), decreasing to
405 0.16 and 0.21, with TFE. While the SMS stress factor has minimal diurnal variability (Fig-
406 ure 4a), PHS features increased stress at midday (Figure 4b), tracking the drop in leaf water
407 potential (Figure 3b,c). Likewise, the PHS stress factor responds to both soil moisture and
408 VPD (Figure 5c,d), while SMS responds only to soil moisture (Figure 5a,b). This results in
409 more wet season (FMA) stress with PHS (as compared to SMS) under both ambient and TFE
410 conditions (Figure 6a-d).

412 ### 5.3 GPP and Transpiration

413 The two models predict similar total GPP across 2002-2003 under TFE, 3.96 kg/m^2
414 (SMS) and 4.00 kg/m^2 (PHS), but GPP is lower for PHS under ambient conditions (4.86
415 kg/m^2) as compared to SMS (5.46 kg/m^2, Figure 6e-h). Seasonal variability in GPP is smaller
416 with PHS. The standard deviations of daily GPP (2002-2003) are 0.49 and 1.55 g/m2/d for
417 AMB/TFE, as compared to 1.53, 2.73 g/m2/d with SMS. Transpiration seasonality is fea-
418 tured in both models (Figure 7a,b), but with a larger amplitude for SMS. PHS yields a better
419 fit to field observations of daily sap flux (see Section zqz), with higher R^2 and lower RMSE
420 compared to SMS under both ambient and TFE conditions (Figure 7c-f).

421 ### 5.4 Root water uptake: dynamics

422 Root water uptake is more sensitive to soil potential with PHS (Figure 8), which fol-
423 lows from sharp declines in hydraulic conductance with drying. Hydraulic conductance de-
424 creases approximately three orders of magnitude across the range of PHS soil potential (Supp
425 Figure A.3b). SMS implied conductance increases with more negative soil potentials, until
426 ψ_{soil} reaches -2.5MPa, beyond which it is defined to equal 0 (Supp Figure A.3a). Root wa-
427 ter uptake still decreases with SMS as soils dry, but due to the decrease in $\Delta\psi$ (Supp Figure
428 A.4c). Whereas PHS imparts a diurnal cycle to root water uptake through dynamic root wa-
429 ter potential, the hydraulic gradient with SMS is defined by ψ_c, which is constant, requiring a
430 diurnal cycle in the implied conductance (Supp Figure A.4).

5.5 Root water uptake: profiles

Overall, the two model configurations feature comparable transpiration during the dry season under ambient conditions (PHS: 28.3cm, SMS: 28.5cm). However they feature distinct vertical profiles, where PHS removes less water from intermediate soil layers (0.5-1.5meters) (Figure 9d). SMS removes more water from these layers, due to the lower sensitivity of root water uptake to soil potential. Likewise partitioning of root water uptake within the soil column is more sensitive to precipitation with PHS (Figure 9a-c). During the longer periods without rain, surface extraction plateaus and transpiration is fueled by the deeper soil water. After rain events, surface extraction renews, while at depth, root water fluxes reverse, with water deposited instead of being extracted. Both models decrease surface extraction under TFE (Figure 9b), but PHS has a larger compensation from beyond 2m (Figure 9c), allowing more overall transpiration (14.6 vs. 10.8 cm).

During the wet season PHS utilizes more water from the near-surface soil layers (Figure 10b), with zero net root water uptake beyond 35.2 cm in ambient conditions (or beyond 9.6cm under TFE). SMS extracts 49.8% (AMB) and 81.5% (TFE) of total transpiration from beyond those levels (Figure 10). PHS does extract farther into the soil profile, but in service of hydraulic redistribution, sending the water deeper into the soil column.

5.6 Hydraulic redistribution

SMS precludes hydraulic redistribution (HR), setting root water uptake to zero when reversed gradients in water potential occur. With PHS, 2003 HR totals to 38.9 cm under ambient conditions and 40.0 cm under TFE, with the majority (28.0, 26.7 cm) occurring at night (Figure 11). HR occurs in both directions (Supp Fig A.5), but is predominately downwards (amb: 30.7cm, tfe: 33.8cm). Likewise HR occurs during both the wet and dry seasons. The seasonality changes with TFE, as AMB has more HR during Sept-Jan, while TFE features more HR during Feb-Apr.

5.7 Soil moisture

During the dry season, SMS simulations yield much lower values for soil matric potential (Figure 12, Supp Fig A.6). During SON, SMS average soil potential is -1.42 MPa under ambient conditions. In lieu of a simple average over the vertical profile, we weight by root-fraction for SMS. For PHS, we use predawn (5AM) root water potential, which best captures the column-effective soil potential (see section zqz). Predawn root water potential averages to -0.14 MPa during SON-2003 under ambient conditions. With TFE, SMS dry season soil potential drops to -2.51 MPa and PHS to -0.50 MPa.

PHS better matches observations, with RMSE lower by up to 55% (Figure 13, Supp Fig A.7). The SMS values correspond to a significant dry bias (Figure 13), especially in the first meter of the soil column. This is associated with the soil wilting parameter (ψ_c), which takes the value -2.5MPa for the broadleaf evergreen tropical PFT [*Oleson et al.*, 2013]. Note that this value is equivalent to the SMS average under TFE in the last paragraph.

5.8 Soil moisture effect on transpiration

Model soil potential shows limited relationship to sap flux observations under ambient conditions (Supp Fig A.8b,f). However, in the SMS configuration, modeled transpiration decreases strongly with more negative soil potential (Supp Fig A.8a), biasing the model relative to observations (Fig 14a).

Sap flux observations under TFE show a stronger relationship with soil potential especially with PHS (Supp Fig A.8h,d). With SMS, the modeled attenuation of transpiration with soil potential again seems to bias modeled transpiration with SMS (Fig 14b). Derived from ψ_c, transpiration approaches zero when soil potential reaches -2.5 MPa (Supp Fig A.8c). The

two PHS simulations feature less structure in transpiration bias vs. soil potential and less bias overall (Fig 14c,d).

6 Discussion

6.1 The promise of plant hydraulics

Plant hydraulics have promised to improve model predictions of vegetation response to climate change [*Sperry and Love*, 2015], especially if parameter ranges and model complexity can be constrained [*Rogers et al.*, 2017]. Numerous site-level models have deployed plant hydraulics (e.g. *Williams et al.* [1996]; *Sperry et al.* [1998]; *Bohrer et al.* [2005]), and studies show vegetation water potential can improve predictions of stomatal response to the environment [*Sperry et al.*, 2017; *Anderegg et al.*, 2017], More recently hydraulics have been coupled to global models [*Bonan et al.*, 2014; *Xu et al.*, 2016; *Christoffersen et al.*, 2016], but most Earth System Models do not provide mechanistic representation of vegetation water dynamics.

In this study, we implement plant hydraulic theory within CLM5, using vegetation water potential to modulate leaf gas exchange and root water uptake. We model water potential according to a simplified circuit analogy (Figure 1), which captures expected diurnal and seasonal dynamics of leaf water potential, with lower values at midday and during the dry season (Figure 3). Our model places the bulk of hydraulic resistance aboveground (Figure 3a), while the added resistance from TFE is primarily from soil-to-root (Figure 3b), consistent with previous results [*Fisher et al.*, 2006]. Need to add a comment that we don't actually match leaf water potential observations very well, but that we didn't tune for that. May add comment on simplifications here, or else add a later section.

Support for hydraulic models cites possible improvements in modeling mortality and productivity [*McDowell et al.*, 2018; *Choat et al.*, 2012]. However, concerns exist in the literature regarding hydraulic model complexity and parameterization [*Verhoef and Egea*, 2014; *Drake et al.*, 2017], which informed our model design (see Section zqz). Recent work suggests model complexity can be managed, given significant coordination of hydraulic traits [*Bartlett et al.*, 2016; *Christoffersen et al.*, 2016]. Likewise incorporating plant hydraulics provides access to new streams of observational data for model validation. Vegetation water potential can be monitored in the field [*Boyer*, 1967] and has been shown to correlate with remote sensing products [*Momen et al.*, 2017]. Parameter values can be measured in the field [*Sack et al.*, 2002] and are available in the TRY database [*Kattge et al.*, 2011].

6.2 Water stress and stomatal conductance

PHS models sunlit and shaded leaf water potential, which serve as the functional input to the water stress factor, replacing the previous version based on soil water potential. This imparts a diurnal cycle to the water stress factor (Figure 4), following the midday drop in leaf water potential. As such, stress now depends on transpiration demand, and, in turn, VPD and solar radiation (Figures 5,A.2). Medlyn does already reduce stomatal conductance based on VPD, but based on A-λE. Here we are trying to impart xylem tension stress, allowing plants to avoid cavitation and embolism. Support for this in the literature [*Novick et al.*, 2016b; *Sperry et al.*, 2017], but still no consensus on the best functional form [*Zhou et al.*, 2013].

The water stress factor follows a seasonal cycle, with lower values (indicating more stress) during the dry season, but with less seasonal variation compared to the control model (Figure 6a-d). As a result PHS features less seasonal variability in GPP, especially under ambient conditions (Figure 6e-h). The xylem tension constraint in PHS imparts a negative feedback on GPP. Factors increasing GPP (e.g. more light) also increase xylem tension and stress, which opposes increases in GPP. *Restrepo-Coupe et al.* [2017] show that GPP in-

creases at Caxiuana during the dry season, suggesting that PHS improves the GPP seasonal cycle relative to the control model.

PHS underestimates the seasonal cycle in transpiration under ambient predictions, with less variability than sap flux observations (Figure 7a,c). We produce a high bias in transpiration under TFE, similar to previous evidence showing that models tend to underestimate the effect of TFE [*Powell et al.*, 2013]. Considerable uncertainty remains regarding the appropriate functional form of water stress. Further work could examine other permutations of water stress, and/or concurrent improvement in photosynthesis parameters and model structure. While a work in progress, PHS does improve transpiration predictions, with lower RMSE and higher correlation compared to the control model, albeit with model tuning (Figure 7).

6.3 The extensive influence of ψ_c

Water stress (in the SMS model configuration) is largely determined by ψ_c, the soil potential with stomates fully closed. For the Broadleaf Evergreen Tropical PFT, ψ_c equals -2.5 MPa [*Oleson et al.*, 2013]. Root water uptake scales with hydraulic gradient ($\Delta\psi$), and ψ_c serves as the sink potential for soil water extraction ($\Delta\psi = \psi_{\text{soil}} - \psi_c$). This defines the slope with which root water uptake decreases with soil drying (Figure 8) and results in transpiration overall trending towards zero as column-average soil potential approaches -2.5 MPa (Supp Fig A.8).

Root water uptake from a given soil layer is defined to be zero whenever soil potential is more negative than ψ_c (Figure 8), following from the definition of the SMS water stress factor (Section zqz). This non-linearity tends to make soil potential decrease to and then hold at ψ_c (Figure 12). As such, ψ_c has strong influence on model output for both transpiration and soil moisture, despite limited empirical or physical basis [*Rogers et al.*, 2017].

6.4 Structural improvements in modeling root water uptake

Using ψ_c is required with SMS, because water potential is not resolved through the vegetation substrate. Instead of a constant parameter, PHS uses dynamic root water potential (ψ_{root}) as the sink for measuring the hydraulic gradient for root water uptake (Figure 3). This provides a critical structural improvement for modeling root water uptake, consistent with extensive evidence of dynamic vegetation water potential (e.g. *Fisher et al.* [2006]). PHS also eschews the constraints on $\Delta\psi$ imposed by SMS (see section zqz).

Root water uptake is equal to the produce of $\Delta\psi$ and the hydraulic conductance. The conductance varies by soil layer and, with PHS, features mechanistic reductions based on root xylem vulnerability and soil hydraulic properties, as is appropriate for hydraulic-based models [*Cai et al.*, 2014; *Warren et al.*]. As a result the soil-root conductance features a strong, positive relationship with soil potential, decreasing almost three orders of magnitude as the soil dries (Supp Fig A.3). PHS k_{sr} appropriately penalizes extraction from depth, due to decreasing root density and increasing xylem length, whereby PHS favors surface extraction when water is available (Figure 10). The model can overcome these penalties, with compensatory root water uptake observed with increased extraction from beyond 2 meters depth during the TFE dry season (Figure 9). Dynamic root water potential (in tandem with declining k) gives the system more play, allowing the model to switch to the lower layers as the surface dries out. PHS allows $\Delta\psi$ to change sign, yielding a representation of hydraulic redistribution, which has been observed in Amazonian forests [*Oliveira et al.*, 2005].

6.5 Hydraulic Redistribution (HR)

During 2003, modeled HR totals to 38.9 cm under ambient conditions and 40.0 cm with TFE (Figure 11). In our simulations, as observed in the field [*Burgess et al.*, 1998], HR occurs in both directions vertically (Supp Fig A.5). Modeled HR is mostly downwards, send-

ing water from rain events deeper into the soil column. This would seem to convey an advantage to deep-rooted individuals, banking water for later use out of reach of shallow-rooted competitors. HR can offer significant water subsidies during dry periods [*Jackson et al.*, 2000] and has been highlighted as an important missing feature in CLM [*Lee et al.*, 2005].

However, there are some challenges with incorporating HR. HR seemed to oversupply the top layer of the soil column (spanning 0 to 2 cm below ground) significantly degraded modeled soil evaporation (not shown). In lieu of this, we set the hydraulic conductance to zero in that uppermost layer, disallowing any root water uptake there. Furthermore observations of HR are extremely difficult, and the degree to which HR actually occurs is unclear. Unequivocal detection of HR involves the observation of reverse flow along transport roots, typically at rates close to the detection threshold of sap flow monitoring systems. In our simulations, HR increases root water uptake by up to 52% relative to transpiration alone (2003, TFE).

HR follows directly from Darcy's Law, occurring when water potential in a given soil layer is more negative than ψ_{root}, but it remains to be seen whether HR as modeled in this implementation is a feature or a liability. PHS may overestimate HR, given the simplified root system architecture [*Bouda and Saiers*, 2017] and the lack of an explicit representation of fine-root cavitation [*Kotowska et al.*, 2015]. Other models, similar to the SMS paradigm, disallow HR by constraining root water uptake to be positive [*Xu et al.*, 2016]. We view this first implementation of HR into the default versions of the CLM as a 'null' hypothesis for the functioning of this process, and as a platform to allow further refinement from the plant hydraulics community.

6.6 Soil moisture and its influence on transpiration

Partly due to HR, vertical and temporal gradients in soil potential are significantly reduced with PHS (Figure 12). This is also related to the root water extraction gradient, which is significantly smaller with PHS (Supp Fig A.4). The SMS sink potential (ψ_c, -2.5MPa), is significantly lower than PHS (ψ_{root}, Figure 3). This is associated with a significant dry bias relative to observations in the SMS simulations, especially in the first meter of the soil column. PHS reduces soil moisture RMSE by up to 55% relative to SMS (Figure 12).

The relationship with soil water potential seems to bias SMS predictions of transpiration relative to sap flux observations (Figure 14). Under ambient conditions, soil water shows little relationship with sap flux observations with either model configuration (Figure A.8b,f), but SMS modeled transpiration decreases strongly in response to soil drying.

7 Conclusion

7.1 Caveats

[need to incorporate this into model description sections]

Modeling stomatal conductance and photosynthesis, especially subject to water stress, is an area of ongoing research. We use the Medlyn model coupled to a hydraulic stress function that attenuates V_{cmax}. This complies with observations [*Lin et al.*, 2018; *Zhou et al.*, 2013] that stress applied through g_1 underestimates attenuation of photosynthesis. However, there is no direct evidence of declines in V_{cmax} with drought [*Flexas et al.*, 2006], whereby future work may seek to represent mesophyll conductance in CLM.

The model hydraulic supply representation is simplified, to reduce the model parameter and computational burdens. No capacitance. No integration of xylem or soil conductances vulnerability, instead based on lower node. No hysteresis in loss of conductance, xylem instantly regain conductance upon re-wetting. Leaf conductance simplified. Soil layers fully parallel, soil potential constant each time step.

Parameter uncertainty is significant. Notions of hydraulic architecture will never perfectly fit on this modeling scale, especially in a PFT paradigm. Field measurements of hydraulic traits will help constrain parameter ranges, but mostly only aboveground. Flux observations can help to tune stress parameters. Parameter estimation for root functioning is significantly more challenging, given the difficulty in underground trait observations. Likewise observational constraints of vertically-resolved states and fluxes underground are scarce. Follow-up work will be geared towards parameter estimation and assessing model skill.

7.2 Utility of modeling vegetation water potential

The PHS configuration of the CLM5 is, to our knowledge, the first Earth System Model with a representation of plant water potential running in its default configuration. In this paper, we have described the model implementation, and illustrated a comparison of the model dynamics for a tropical rainforest site subjected to water limitation, given that prediction of rainforest responses to drought is one of the key uncertainties in the ESM predictions. Overall, the new model behaviour differs from the default configuration in ways that are expected, given its structural properties, and in many cases, provides better correspondance with the observations that the default structure.

In this paper, however, we do not undertake a comprehensive assessment of which model structure performs better, given the substantial parametric uncertainty in both models, and the dependence on numerous other features of the CLM external to water stress representation that contribute to model-observation divergences - in this case in particular, the overestimation of unstressed transpiration by both versions of the model compared to the observations.

In lieu of this type of assessment, we propose that the new PHS model structure 1) is more closely aligned with known plant hydraulics theory, 2) provides significantly improved connections to real-world observational data streams (of leaf and stem water status, sap flow, percent loss conductance) and 3) represents known features of ecohydrological function that the default model cannot capture, including hydraulic redistribution, changes in the depth of water uptake with drought stress, plant embolism impacts on gas exchange and responses of water uptake to changes in leaf:root rations.

This will be the final conclusions. Any comments on overall takeaways?

PHS models vegetation water potential. This offers structural improvements for stress and for root water uptake. Stress now functions with hydraulic limitation.

8 Acknowledgments

9 Figures

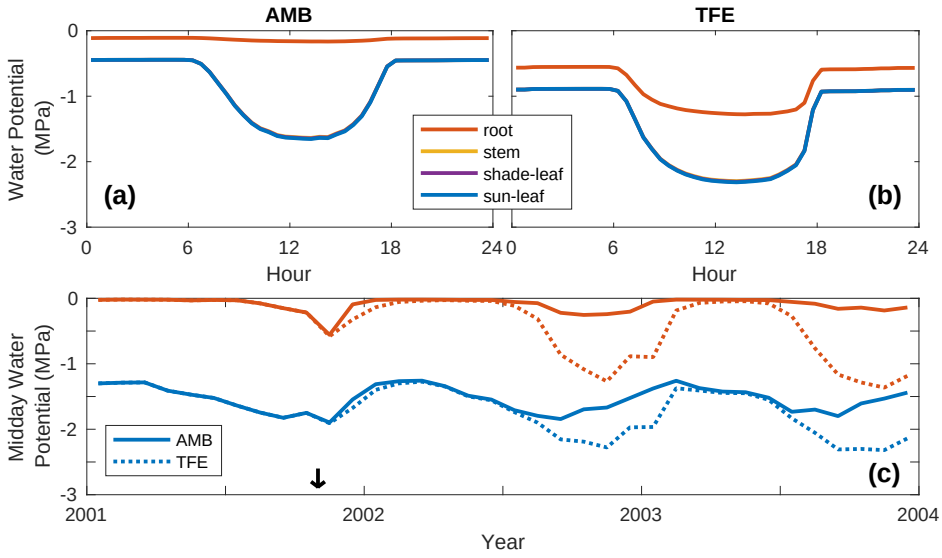

Figure 3. Modeled vegetation water potential at Caxiuanã, Brazil. (a) 2003 dry season (SON) diurnal mean, ambient through-fall conditions, (b) 2003 dry season diurnal mean, with 60% TFE. Curves are drawn for sunlit leaf, shaded leaf, stem, and root water potentials, with the latter three overlapping. (c) Monthly average midday (12h-14h) root and leaf water potential, under ambient (solid line) and TFE (dotted line) conditions. Note that TFE begins Nov 1, 2001, as indicated by the vertical arrow.

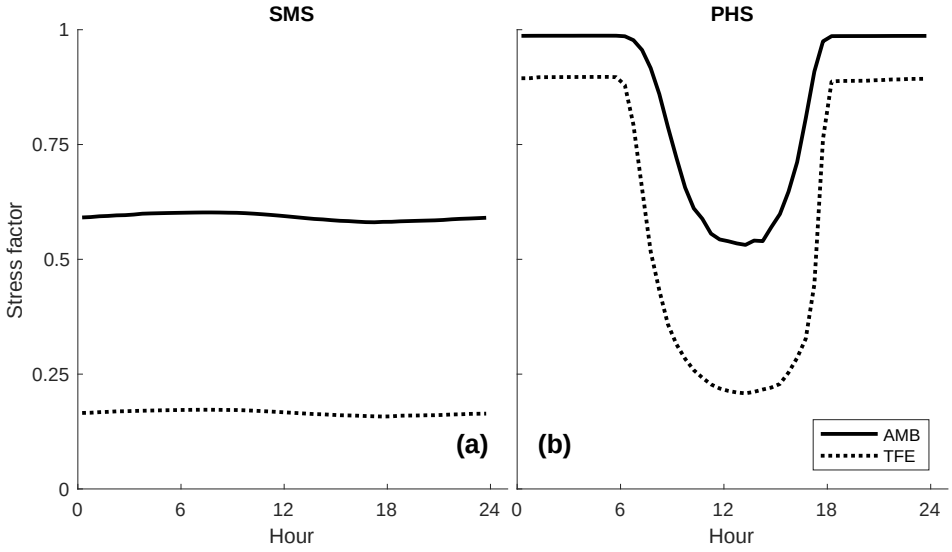

659 **Figure 4.** 2003 dry season (SON) diurnal mean water stress function for (a) SMS, and (b) PHS. Note that
660 the water stress factor equals 1 when there is no stress and 0 when fully stressed.

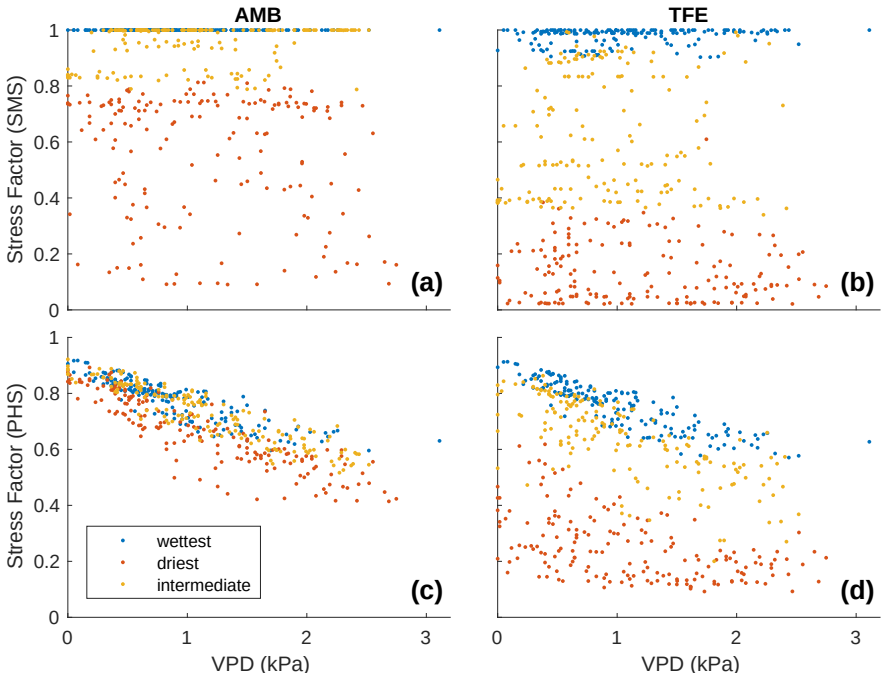

Figure 5. Water stress factor versus vapor pressure deficit (2002-2003), for timesteps with downwelling shortwave radiation between 400 and 425 W/m2 (n=515). Radiation is controlled to highlight the relationship with VPD, the reverse (controlling for VPD) is shown in Figure A.2. For SMS (a,b), data are subdivided based on average soil matric potential, weighted by root fraction. For PHS (c,d), data are subdivided based on predawn (5h) root water potential. Blue dots represent the wettest tercile, yellow dots represent the intermediate tercile, and red dots represent the driest tercile (see Table 2).

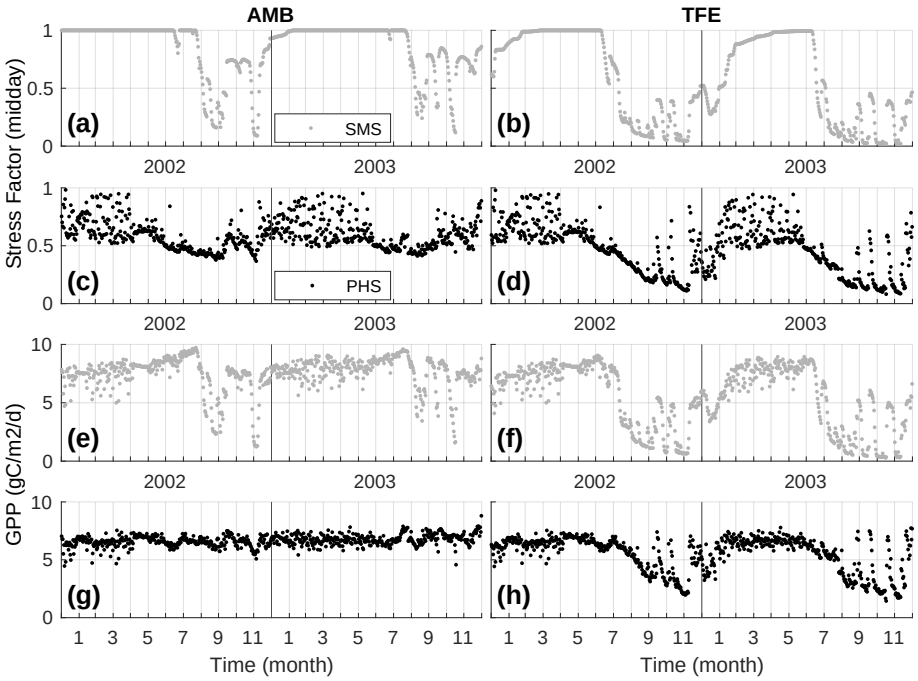

667 **Figure 6.** Daily stress factor (midday, averaged over 12h-14h) and GPP during 2002-2003 under ambient
668 (left) and TFE (right) conditions. Output from the SMS configuration (a,b,e,f) are plotted with gray color,
669 while output from the PHS configuration (c,d,g,h) are plotted in black.

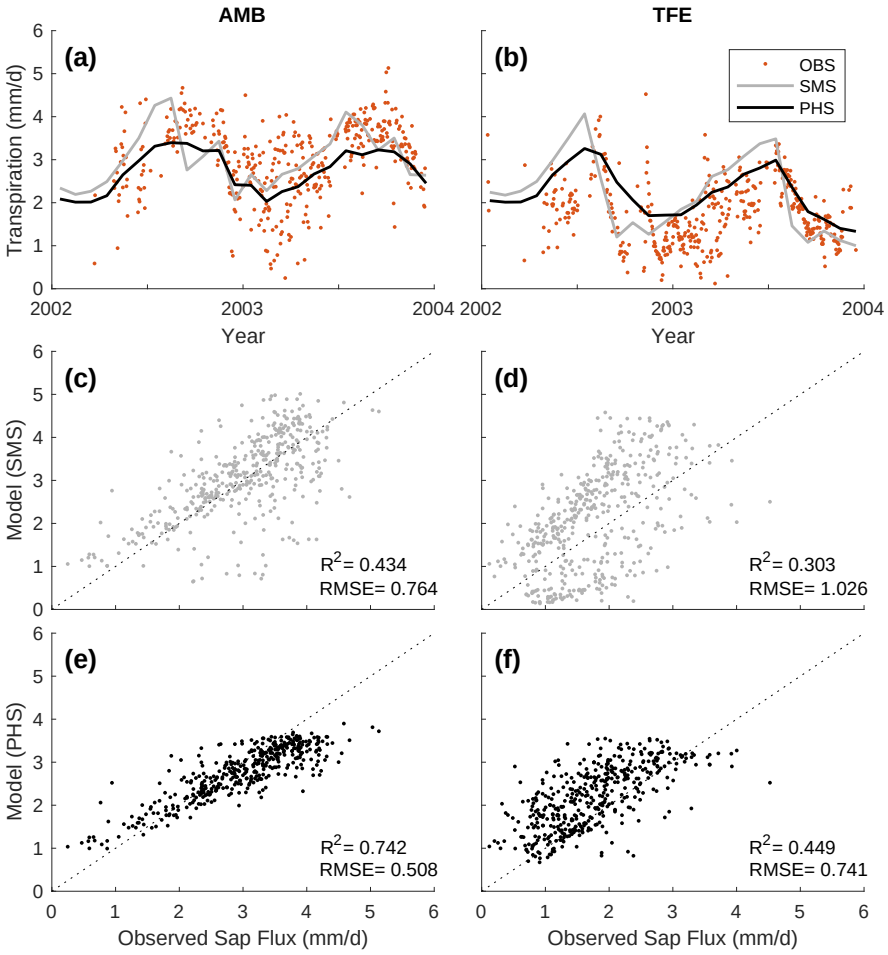

Figure 7. (a,b) Monthly mean water stress function. The water stress factor equals 1 when there is no stress and 0 when fully stressed. (c,d) Monthly mean transpiration (W/m^2). (e,f) Monthly mean gross primary productivity ($g/m^2/d$). Solid lines correspond to ambient through-fall conditions, and dotted lines feature 60% through-fall exclusion. Black lines represent model output. Red lines show observational transpiration derived from sap flux (see zqz). PHS is on for (a), (c), and (e). PHS is off for (b), (d), and (f).

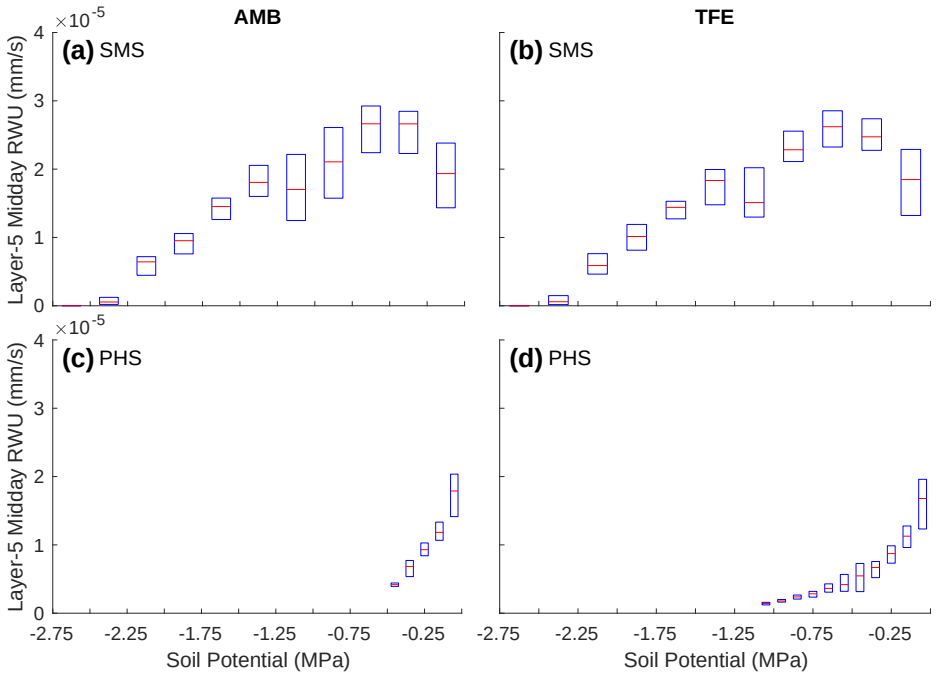

Figure 8. Binned boxplot of root water uptake versus soil potential for Soil Layer 5 (2002-3). Red lines mark the median, with boxes spanning the interquartile range. Bin sizes are 0.25 MPa for SMS and 0.1 MPa for PHS. Soil Layer 5 is shown, because it is near the surface (20 to 32 cm) and has a large root fraction (14.4%). Only midday (12h-14h) timesteps are shown to highlight the relationship with soil potential.

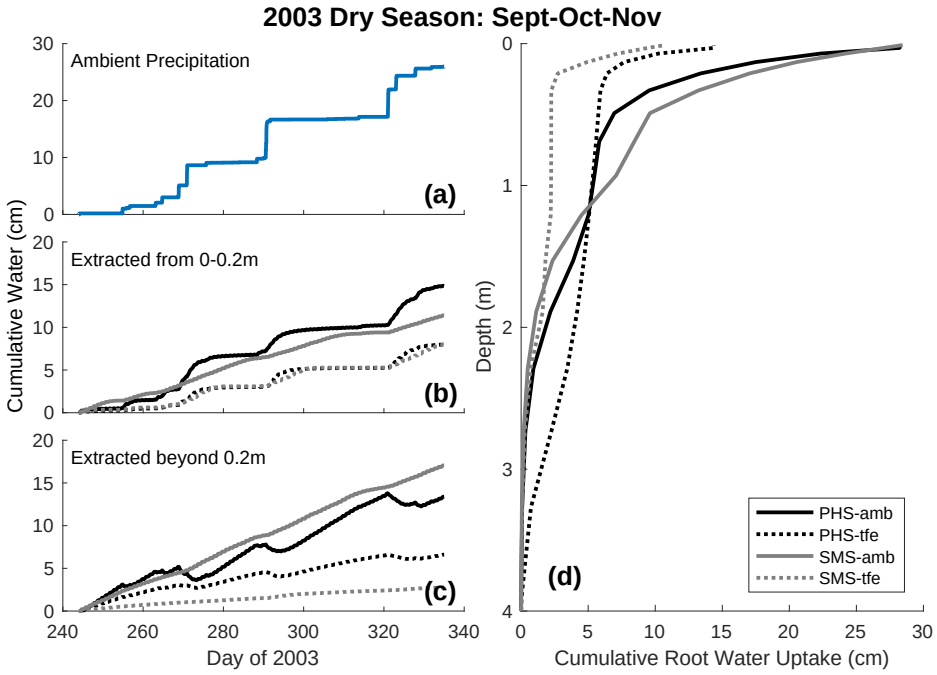

Figure 9. 2003 dry season (SON) cumulative root water uptake and precipitation. (a) Cumulative root water uptake with depth across the four simulations. (b,c) Cumulative water uptake over time from above and below 0.2m, respectively. (d) Cumulative precipitation under ambient conditions.

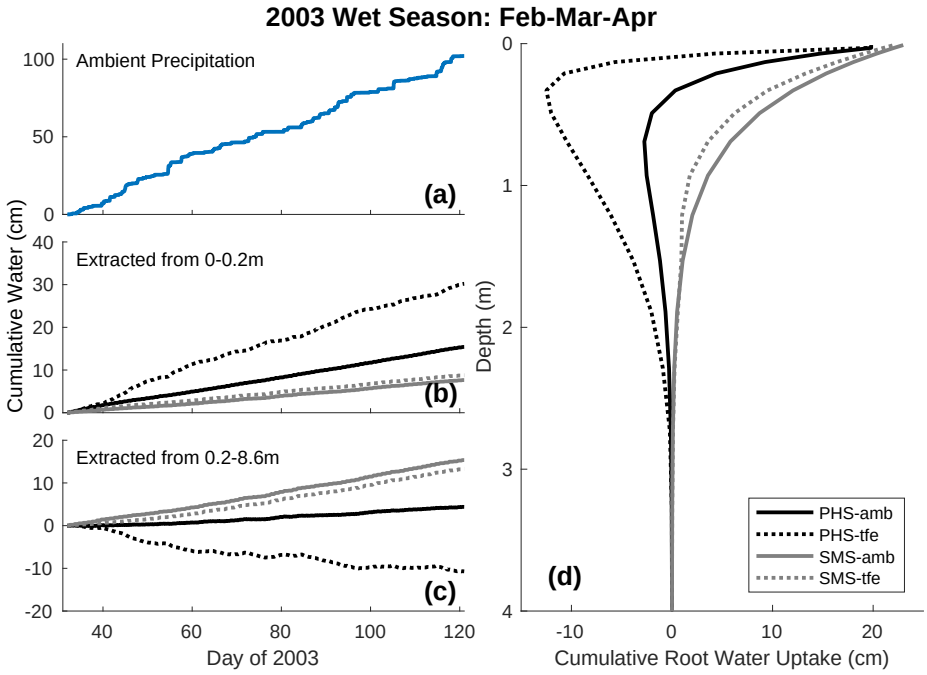

682 **Figure 10.** 2003 wet season (FMA) cumulative root water uptake and precipitation. (a) Cumulative root
683 water uptake with depth across the four simulations. (b,c) Cumulative water uptake over time from above and
684 below 0.2m, respectively. (d) Cumulative precipitation under ambient conditions.

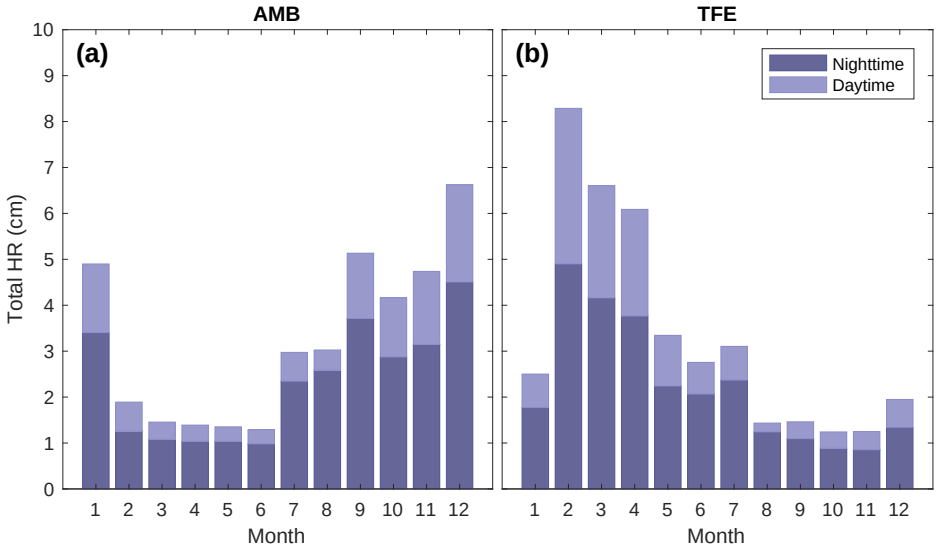

685 **Figure 11.** Total hydraulic redistribution (cm) by month across in 2003. For (a) ambient through-fall con-
686 ditions, and (b) 60% through-fall exclusion. Darker shading shows portion of HR at night [6pm,6am), lighter
687 shading shows portion of HR during day [6am,6pm). Total HR refers to the sum of all negative root water
688 uptake flows, where water is deposited by roots into a given soil layer.

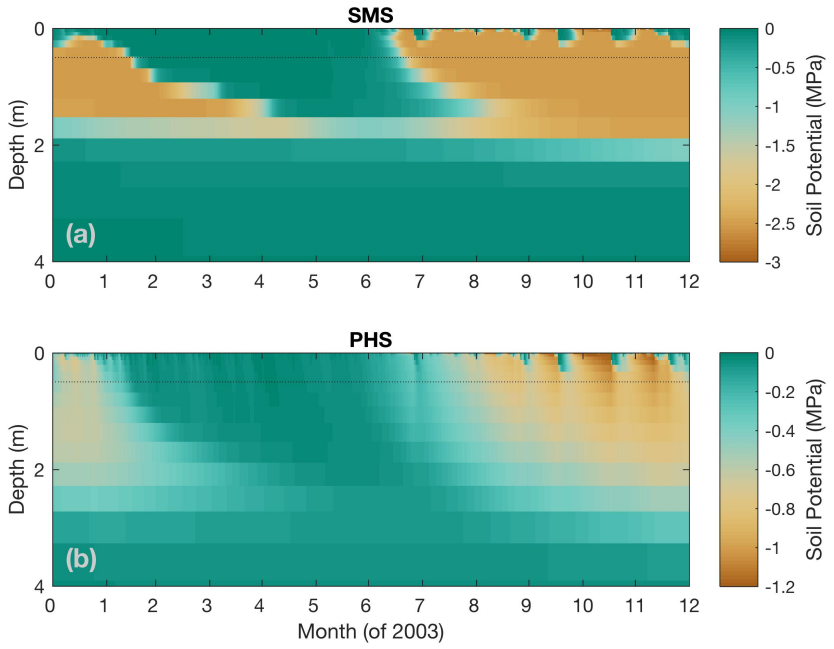

689 **Figure 12.** Vertical profile of soil water potential (MPa) over time under 60% through-fall exclusion, for
690 (a) SMS, and (b) PHS. Note that color axes are different. SMS soil potential spends long periods at -2.5MPa,
691 which is the value of parameter ψ_c. Figure 13 subsets this data at 0.5m depth (dotted line), plotted alongside
692 observations. Soil potential under ambient conditions is shown in Supp Fig A.6.

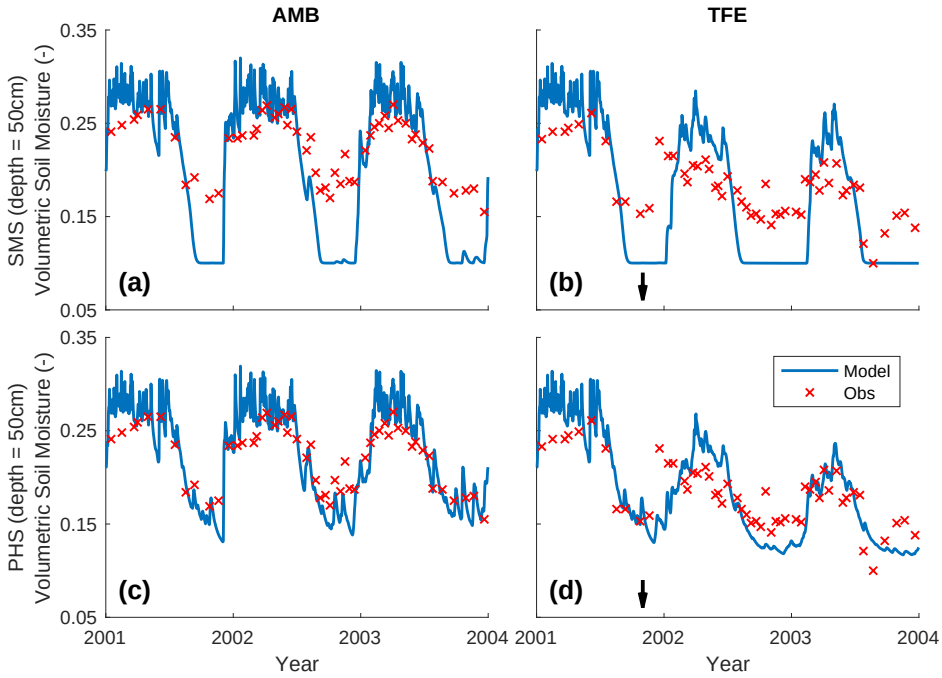

693 **Figure 13.** Volumetric soil moisture (-) over time under ambient and TFE conditions at depth of 50cm.
694 (a/b) SMS (c/d) PHS. RMSE are 0.048, 0.049, 0.022, and 0.029. Arrows indicate start of TFE. Figure A.7
695 shows the same plots at 7 other soil depths.

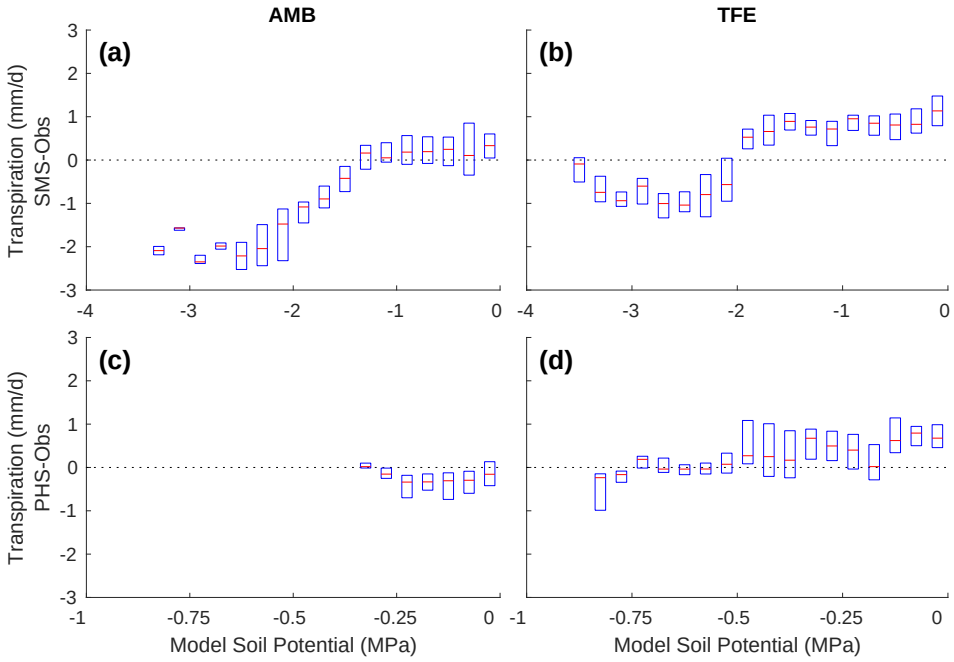

Figure 14. Binned boxplot showing the difference between modeled and observed transpiration (mm/d) versus model soil potential. Red lines are drawn at the median, with boxes spanning the interquartile range. The two models use different root water uptake paradigms, from which we define different operators for column effective soil potential. For SMS we average over the soil column weighted by root fraction and over time (daily mean). For PHS we use predawn (5h) root water potential. Bin widths are 0.2 MPa for SMS (a,b) and 0.05 MPa for PHS (c,d).

A: Supplementary Figures

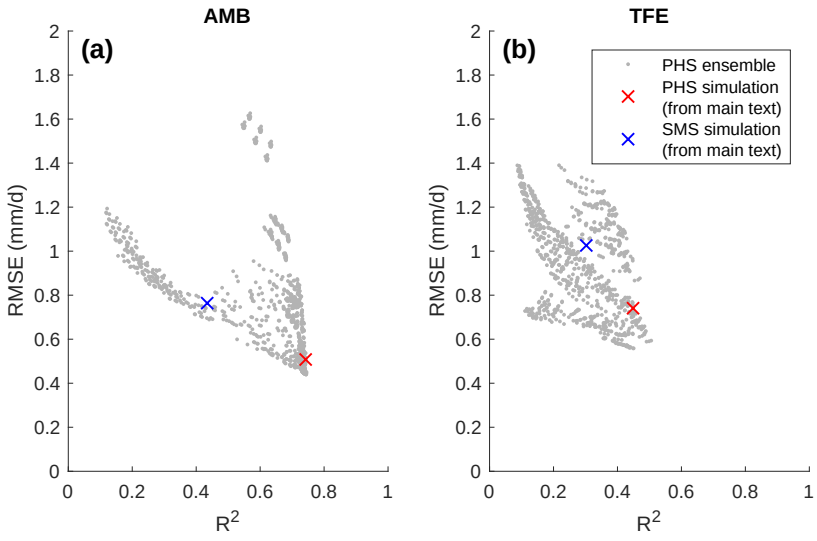

Figure A.1. Parameter tuning exercise.

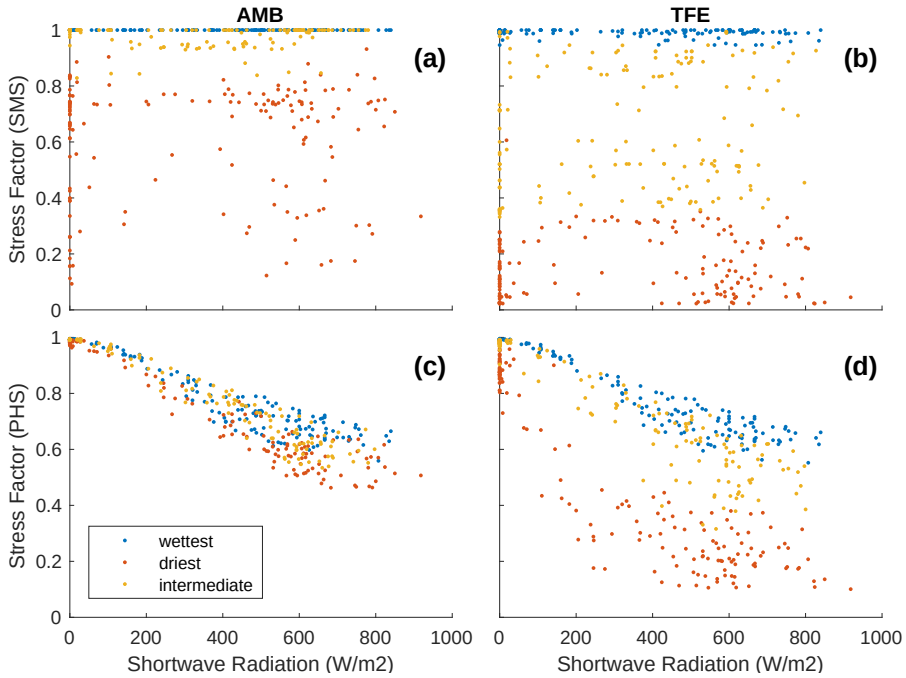

Figure A.2. Water stress factor versus downwelling shortwave radiation (2002-2003), for timesteps with VPD between 1 and 1.0559 kPa (n=470). VPD is controlled to highlight the relationship with downwelling radiation, the reverse (controlling for radiation) is shown in Figure 5. For SMS (a,b), data are subdivided based on average soil matric potential, weighted by root fraction. For PHS (c,d), data are subdivided based on predawn (5h) root water potential. Blue dots represent the wettest tercile, yellow dots represent the intermediate tercile, and red dots represent the driest tercile.

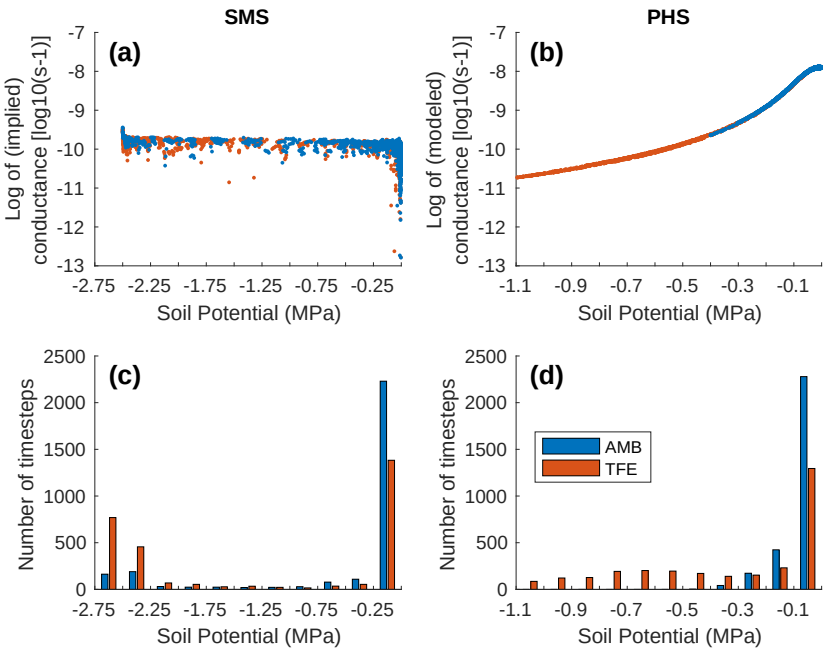

Figure A.3. Log of conductance versus soil potential for Soil Layer 5 (2002-3). Only midday (12h-14h) timesteps are shown to emphasize the relationship with soil potential. With SMS, conductance is not modeled explicitly, but rather calculated as $k{=}q/\Delta\psi$ (see Section zqz). Beyond 2.5MPa, SMS implied conductance equals 0. PHS conductance captures both root tissue and soil matrix resistances (operating in series).

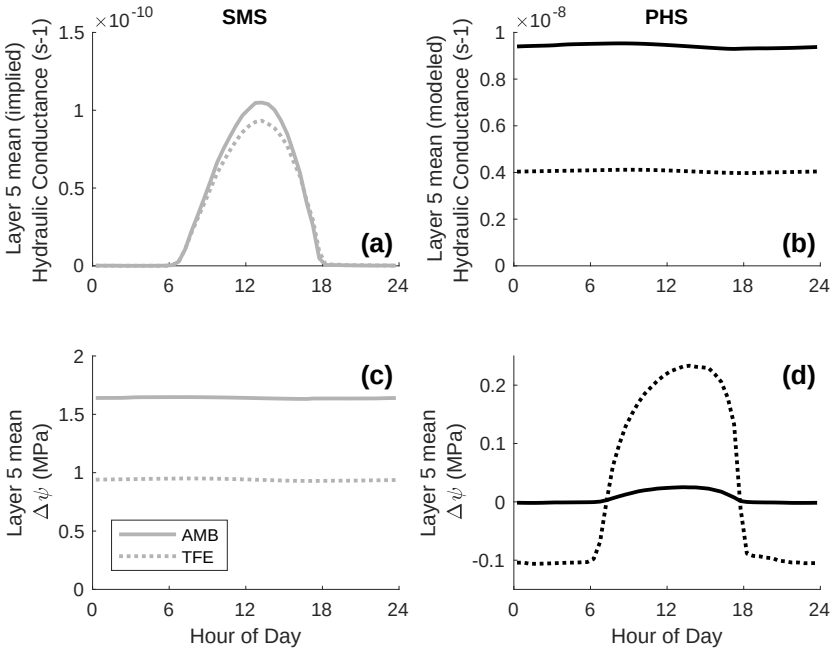

714 **Figure A.4.** 2003 diurnal mean of Soil Layer 5 conductance and $\Delta\psi$, under ambient and TFE conditions.

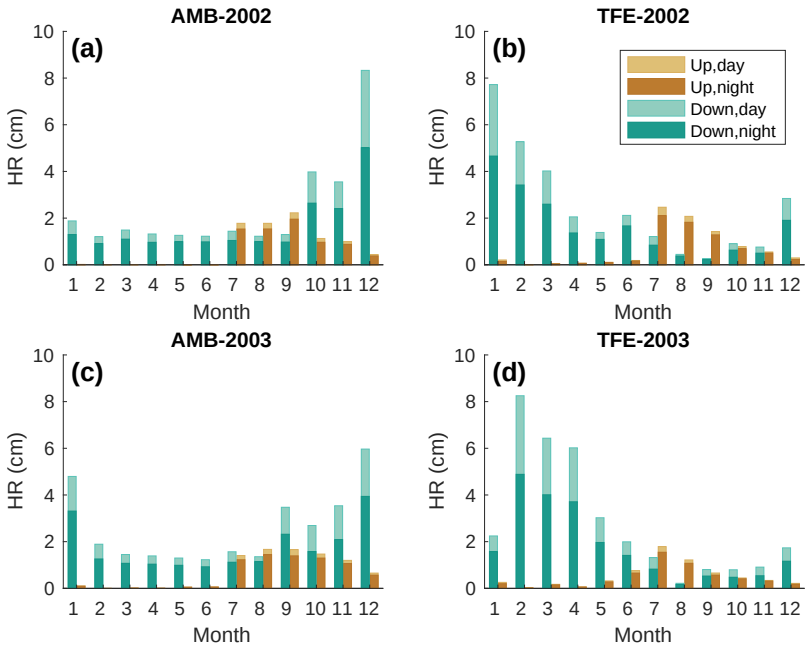

Figure A.5. PHS hydraulic distribution during 2003. Alternative version partitioning by direction.

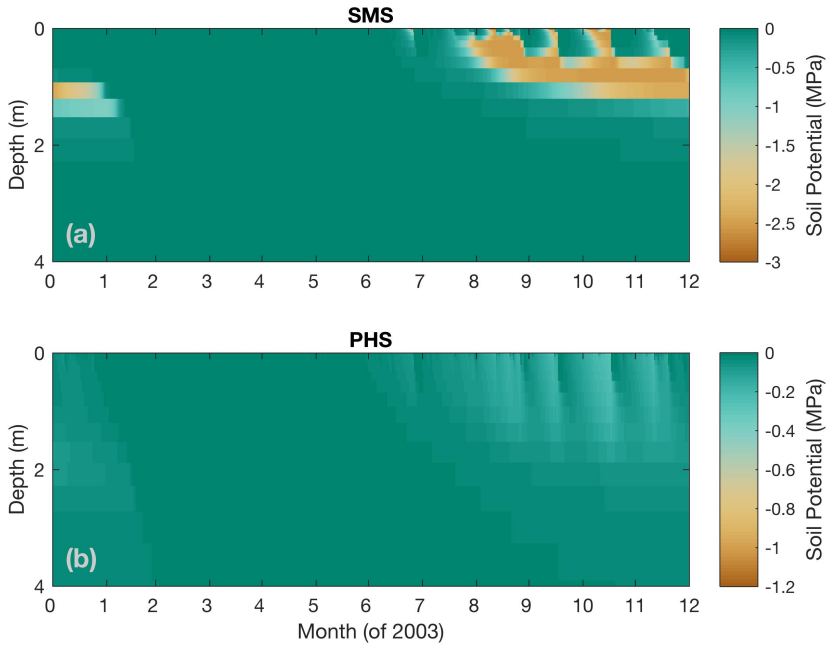

716 **Figure A.6.** Vertical profile of soil water potential (MPa) through time under ambient through-fall condi-
717 tions, for (a) PHS, and (b) SMS. Note that color axes are different.

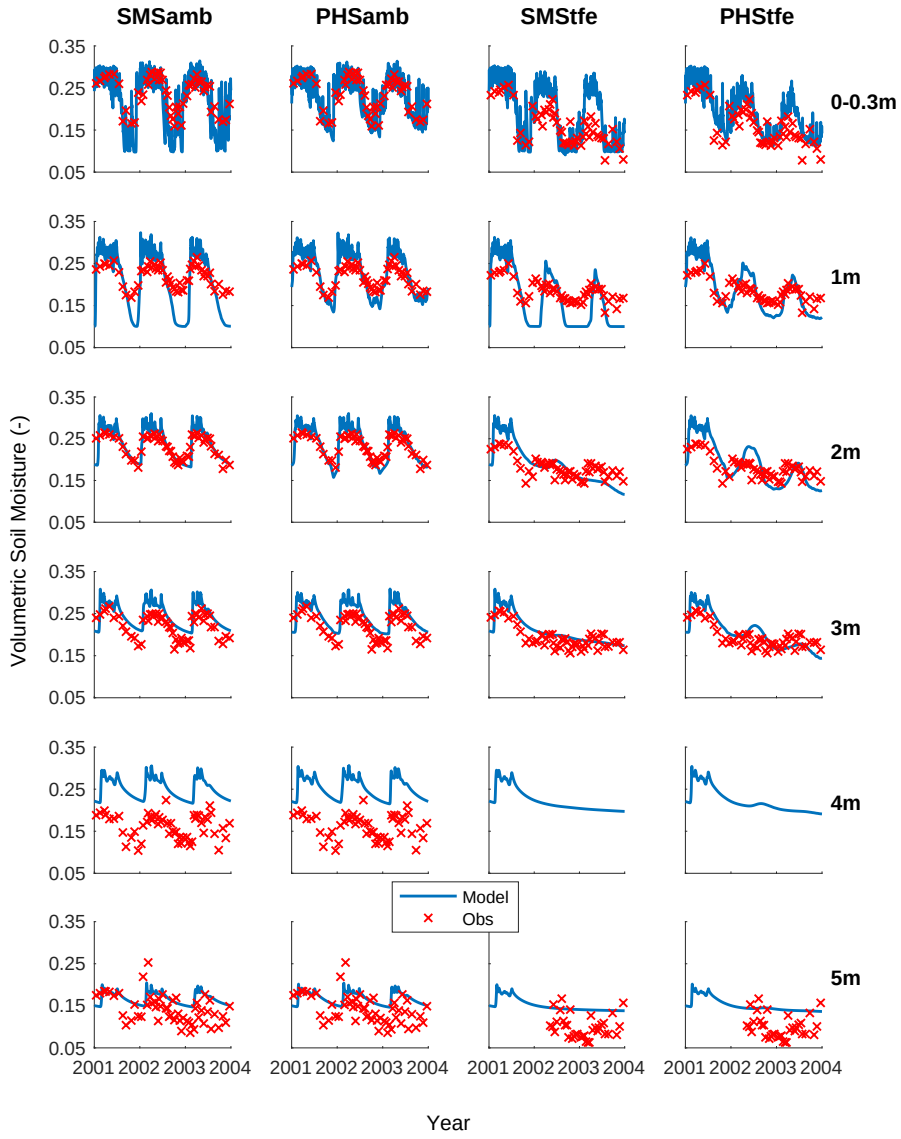

718 **Figure A.7.** Time series of soil moisture by soil layer. Complements Figure 12

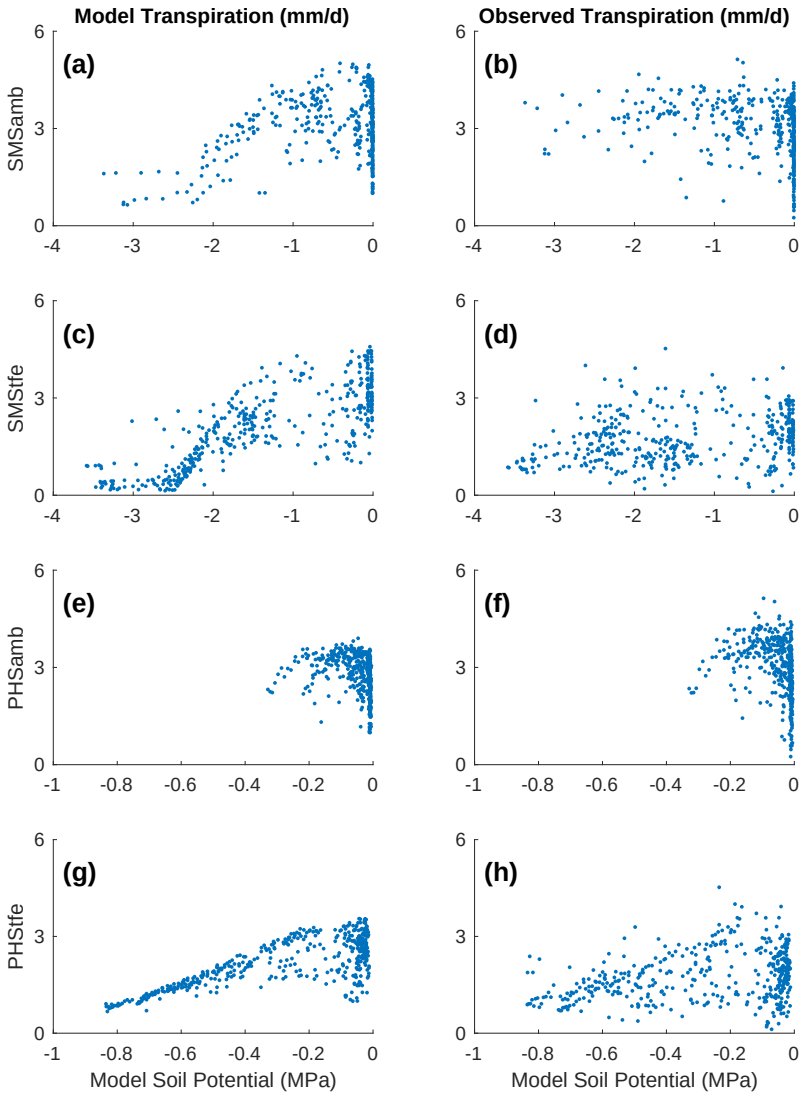

719 **Figure A.8.** Modeled (left column) and observed (right column) transpiration vs. model soil potential.
720 Complements Figure 14

B: Appendix to Model Description

B.1 Details of Water Supply

PHS resolves flow across four different segments, soil-to-root, root-to-stem, stem-to-leaf, and leaf-to-transpiration.

Stem-to-leaf. The area bases are sunlit and shaded leaf area, respectively. Note that gravity is assumed negligible here. Likewise there is no length scaling applied to maximum conductance. Therefore the input parameters for $k_{1,\max}$ should be conductances (s^{-1}).

$$\begin{aligned} q_{1a} &= k_1 \cdot \text{LAI-sun} \cdot (\psi_{\text{stem}} - \psi_{\text{sun-leaf}}) \\ q_{1b} &= k_1 \cdot \text{LAI-shade} \cdot (\psi_{\text{stem}} - \psi_{\text{shade-leaf}}) \end{aligned} \tag{B.1}$$

$$k_1 = k_{1,\max} \cdot f\left(\psi_{\text{stem}}\right) \tag{B.2}$$

$$f\left(\psi\right) = 2^{-\left(\frac{\psi}{p_{50}}\right)^{c_k}} \tag{B.3}$$

Root-to-stem. The area basis is stem area index. The parameter is maximum stem xylem conductivity ($K_{2,\max}$). Stem conductance (k_2) is the result of scaling maximum conductivity by the tree height (h) and applying loss relative to maximum conductance via the vulnerability curve $f\left(\psi_{\text{root}}\right)$.

$$q_2 = k_2 \cdot \text{SAI} \cdot (\psi_{\text{root}} - \psi_{\text{stem}} - \rho g h) \tag{B.4}$$

$$k_2 = \frac{K_{2,\max}}{h} \cdot f\left(\psi_{\text{root}}\right) \tag{B.5}$$

Soil-to-root. Area basis is RAI in soil layer i, which is based on the layer root fraction times the total root area. Total root area we have as the summed stem and leaf area indices multiplied by a relative root area parameter (f_{root}). The vertical root distribution is defined by the layer root fraction (r_i), which follows a one-parameter (by PFT) power law decay following *Jackson et al.* [1996].

$$q_{3,i} = k_{3,i} \cdot \text{RAI}_i \cdot (\psi_{\text{soil,i}} - \psi_{\text{root}} - \rho g z_i) \tag{B.6}$$

$$\text{RAI}_i = f_{\text{root}} \cdot (\text{SAI} + \text{LAI}) \cdot r_i \tag{B.7}$$

$$k_{3,i} = \frac{k_{r,i} + k_{s,i}}{k_{r,i} \cdot k_{s,i}} \tag{B.8}$$

$$k_{r,i} = \frac{K_{r,\max}}{l_i} f\left(\psi_{\text{soil,i}}\right) \tag{B.9}$$

$$l_i = z_i + x \tag{B.10}$$

$$k_{s,i} = \frac{K_{s,i}}{d} \tag{B.11}$$

The conductance $k_{3,i}$ reflects two resistors in series, from soil-to-root ($k_{s,i}$) and through the root tissue ($k_{r,i}$). The root tissue conductance is attenuated via the vulnerability curve framework. The input parameter is maximum root xylem conductivity, on the basis of RAI as defined above. The root conductivity is scaled by the conducting length, which is estimated as the sum of soil layer depth (z_i) and average lateral extent (x, static parameter). The soil conductivity $K_{s,i}$ is calculated from the layer soil matric potential (ψ_s) and soil properties following *Clapp and Hornberger* [1978] as described in *Oleson et al.* [2013]. The soil conductance ($k_{s,i}$) is the result of scaling the conductivity by d, the distance between roots estimated following *Williams et al.* [1996] and *Bonan et al.* [2014]

The challenge here is obviously getting your head around all the parameters.

B.2 Details of Water Demand

B.3 Details of Solution

The continuity of water flow through the system yields four equations

$$\begin{aligned} E_{sun} &= q_{1a} \\ E_{shade} &= q_{1b} \\ q_{1a} + q_{1b} &= q_2 \\ q_2 &= \sum_{i=1}^{nlevsoi} q_{3,i} \end{aligned} \tag{B.12}$$

We seek the set of vegetation water potential values (four unknowns),

$$\psi = \begin{bmatrix} \psi_{sunleaf} \\ \psi_{shadeleaf} \\ \psi_{stem} \\ \psi_{root} \end{bmatrix} \tag{B.13}$$

that satisfies these equations, as forced by the soil moisture and atmospheric state.

Each flux on the schematic can be represented in terms of the relevant water potentials.

Defining the transpiration fluxes:

$$\begin{aligned} E_{sun} &= E_{sun,max} \cdot 2^{-\left(\frac{\psi_{sunleaf}}{p50_e}\right)^{c_k}} \\ E_{shade} &= E_{shade,max} \cdot 2^{-\left(\frac{\psi_{shadeleaf}}{p50_e}\right)^{c_k}} \end{aligned} \tag{B.14}$$

Defining the water supply fluxes:

$$\begin{aligned} q_{1a} &= k_{1a,max} \cdot 2^{-\left(\frac{\psi_{stem}}{p50_1}\right)^{c_k}} \cdot \mathrm{LAI}_{sun} \cdot \left(\psi_{stem} - \psi_{sunleaf}\right) \\ q_{1b} &= k_{1b,max} \cdot 2^{-\left(\frac{\psi_{stem}}{p50_1}\right)^{c_k}} \cdot \mathrm{LAI}_{shade} \cdot \left(\psi_{stem} - \psi_{shadeleaf}\right) \\ q_2 &= \frac{k_{2,max}}{z_2} \cdot 2^{-\left(\frac{\psi_{root}}{p50_2}\right)^{c_k}} \cdot SAI \cdot (\psi_{root} - \psi_{stem} - \Delta\psi_z) \\ q_{soil} &= \sum_{i=1}^{nlevsoi} q_{3,i} = \sum_{i=1}^{nlevsoi} k_{3,i} \cdot RAI \cdot (\psi_{soil,i} - \psi_{root} + \Delta\psi_{z,i}) \end{aligned} \tag{B.15}$$

We're looking to find the vector ψ that fits with soil and atmospheric forcings while satisfying water flow continuity. Due to the model non-linearity, we use a linearized explicit approach, iterating with Newton's method. The initial guess is the solution for ψ (vector) from the previous time step. The general framework, from iteration m to $m + 1$ is:

$$\begin{aligned} q^{m+1} &= q^m + \frac{\delta q}{\delta \psi}\Delta\psi \\ \psi^{m+1} &= \psi^m + \Delta\psi \end{aligned} \tag{B.16}$$

So for our first flux balance equation, at iteration $m + 1$, we have:

$$E_{sun}^{m+1} = q_{1a}^{m+1} \tag{B.17}$$

Which can be linearized to:

$$E_{sun}^{m} + \frac{\delta E_{sun}}{\delta \psi}\Delta\psi = q_{1a}^{m} + \frac{\delta q_{1a}}{\delta \psi}\Delta\psi \tag{B.18}$$

And rearranged to be:

$$\frac{\delta q_{1a}}{\delta \psi}\Delta\psi - \frac{\delta E_{sun}}{\delta \psi}\Delta\psi = E_{sun}^{m} - q_{1a}^{m} \tag{B.19}$$

And for the other 3 flux balance equations:

$$\begin{aligned} \frac{\delta q_{1b}}{\delta \psi}\Delta\psi - \frac{\delta E_{sha}}{\delta \psi}\Delta\psi &= E_{sha}^{m} - q_{1b}^{m} \\ \frac{\delta q_{2}}{\delta \psi}\Delta\psi - \frac{\delta q_{1a}}{\delta \psi}\Delta\psi - \frac{\delta q_{1b}}{\delta \psi}\Delta\psi &= q_{1a}^{m} + q_{1b}^{m} - q_{2}^{m} \\ \frac{\delta q_{soil}}{\delta \psi}\Delta\psi - \frac{\delta q_{2}}{\delta \psi}\Delta\psi &= q_{2}^{m} - q_{soil}^{m} \end{aligned} \tag{B.20}$$

Putting all four together in matrix form:

$$\begin{bmatrix} \frac{\delta q_{1a}}{\delta \psi} - \frac{\delta E_{sun}}{\delta \psi} \\ \frac{\delta q_{1b}}{\delta \psi} - \frac{\delta E_{sha}}{\delta \psi} \\ \frac{\delta q_{2}}{\delta \psi} - \frac{\delta q_{1a}}{\delta \psi} - \frac{\delta q_{1b}}{\delta \psi} \\ \frac{\delta q_{soil}}{\delta \psi} - \frac{\delta q_{2}}{\delta \psi} \end{bmatrix} \Delta\psi = \begin{bmatrix} E_{sun}^{m} - q_{1a}^{m} \\ E_{sha}^{m} - q_{1b}^{m} \\ q_{1a}^{m} + q_{1b}^{m} - q_{2}^{m} \\ q_{2}^{m} - q_{soil}^{m} \end{bmatrix} \tag{B.21}$$

Now to expand the left-hand side, from vector ψ to the four distinct plant water potential nodes, noting that many derivatives are zero (e.g. $\frac{\delta E_{sun}}{\delta \psi_{sha}} = 0$)

Introducing the notation: $A\Delta\psi = b$

$$\Delta\psi = \begin{bmatrix} \Delta\psi_{sunleaf} \\ \Delta\psi_{shadeleaf} \\ \Delta\psi_{stem} \\ \Delta\psi_{root} \end{bmatrix} \tag{B.22}$$

$$A = \begin{bmatrix} \frac{\delta q_{1a}}{\delta \psi_{sun}} - \frac{\delta E_{sun}}{\delta \psi_{sun}} & 0 & \frac{\delta q_{1a}}{\delta \psi_{stem}} & 0 \\ 0 & \frac{\delta q_{1b}}{\delta \psi_{sha}} - \frac{\delta E_{sha}}{\delta \psi_{sha}} & \frac{\delta q_{1b}}{\delta \psi_{stem}} & 0 \\ -\frac{\delta q_{1a}}{\delta \psi_{sun}} & -\frac{\delta q_{1b}}{\delta \psi_{sha}} & \frac{\delta q_{2}}{\delta \psi_{stem}} - \frac{\delta q_{1a}}{\delta \psi_{stem}} - \frac{\delta q_{1b}}{\delta \psi_{stem}} - \frac{\delta q_{2}}{\delta \psi_{stem}} & \frac{\delta q_{2}}{\delta \psi_{root}} \\ 0 & 0 & \frac{\delta q_{soil}}{\delta \psi_{root}} - \frac{\delta q_{2}}{\delta \psi_{root}} & \end{bmatrix} \tag{B.23}$$

$$b = \begin{bmatrix} E^m_{sun} - q^m_{b1} \\ E^m_{sha} - q^m_{b2} \\ q^m_{b1} + q^m_{b2} - q^m_{stem} \\ q^m_{stem} - q^m_{soil} \end{bmatrix} \tag{B.24}$$

Now we compute all the entries for A and b based on the soil moisture and maximum transpiration forcings and can solve to find:

$$\Delta\psi = A^{-1} b \tag{B.25}$$

$$\psi_{m+1} = \psi_m + \Delta\psi \tag{B.26}$$

We iterate until $b \to 0$, signifying water flux balance through the system. The result is a final set of water potentials ($\psi_{root}, \psi_{xylem}, \psi_{shadeleaf}, \psi_{sunleaf}$) satisfying non-divergent water flux through the system. The magnitude of the water flux is driven by soil matric potential and unstressed ($\beta_t = 1$) transpiration.

We use the transpiration solution (corresponding to the final solution for ψ) to compute stomatal conductance. The stomatal conductance is then used to compute β_t.

$$\beta_{t,sun} = \frac{g_{s,sun}}{g_{s,sun,\beta_t=1}} \tag{B.27}$$

$$\beta_{t,shade} = \frac{g_{s,shade}}{g_{s,shade,\beta_t=1}} \tag{B.28}$$

The β_t values are used in the Photosynthesis module (see section 2.1) to apply water stress. The solution for ψ is saved as a new variable (vegetation water potential) and is indicative of plant water status. The soil-to-root fluxes $(q_{3,1}, q_{3,2}, ..., q_{3,n})$ are used as the soil transpiration sink in the Richards' equation subsurface flow equations.

Furthermore several simplifications were made that decrease the numerical complexity. For the purposes of the PHS solution, soil potentials are assumed constant during each timestep. Plant tissue water storage (capacitance) is not represented, whereby the solution does not depend on the previous timestep and has no time derivatives.

Acknowledgments

= enter acknowledgments here =

PIerre: Text I removed While there are disagreements about soil moisture trends globally [*Dai*, 2013; *Sheffield et al.*, 2012], Amazonia has experienced and a lengthening dry season [*Fu et al.*, 2013] and faces projections of increasing frequency of extreme El Niño events [*Cai et al.*, 2014]

References

Allen, C. D., A. K. Macalady, H. Chenchouni, D. Bachelet, N. McDowell, M. Vennetier, T. Kitzberger, A. Rigling, D. D. Breshears, E. T. Hogg, P. Gonzalez, R. Fensham, Z. Zhang, J. Castro, N. Demidova, J.-H. Lim, G. Allard, S. W. Running, A. Semerci, and N. Cobb (2010), A global overview of drought and heat-induced tree mortality reveals emerging climate change risks for forests, *Forest Ecology and Management*, *259*(4), 660 – 684, doi:https://doi.org/10.1016/j.foreco.2009.09.001.

Anderegg, W. R. L. (2015a), Spatial and temporal variation in plant hydraulic traits and their relevance for climate change impacts on vegetation, *New Phytologist*, *205*(3), 1008–1014, doi:10.1111/nph.12907.

Anderegg, W. R. L., J. M. Kane, and L. D. L. Anderegg (2013a), Consequences of widespread tree mortality triggered by drought and temperature stress, *Nature Climate Change*, *3*(1), 30–36.

Anderegg, W. R. L., L. Plavcová, L. D. L. Anderegg, U. G. Hacke, J. A. Berry, and C. B. Field (2013b), Drought's legacy: multiyear hydraulic deterioration underlies widespread aspen forest die-off and portends increased future risk, *Global Change Biology*, *19*(4), 1188–1196, doi:10.1111/gcb.12100.

Anderegg, W. R. L., C. Schwalm, F. Biondi, J. J. Camarero, G. Koch, M. Litvak, K. Ogle, J. D. Shaw, E. Shevliakova, A. P. Williams, A. Wolf, E. Ziaco, and S. Pacala (2015b), Pervasive drought legacies in forest ecosystems and their implications for carbon cycle models, *Science*, *349*(6247), 528–532, doi:10.1126/science.aab1833.

Anderegg, W. R. L., A. Wolf, A. Arango-Velez, B. Choat, D. J. Chmura, S. Jansen, T. Kolb, S. Li, F. Meinzer, P. Pita, V. Resco de Dios, J. S. Sperry, B. T. Wolfe, and S. Pacala (2017), Plant water potential improves prediction of empirical stomatal models, *PLOS ONE*, *12*(10), 1–17, doi:10.1371/journal.pone.0185481.

Bartlett, M. K., T. Klein, S. Jansen, B. Choat, and L. Sack (2016), The correlations and sequence of plant stomatal, hydraulic, and wilting responses to drought, *Proceedings of the National Academy of Sciences*, *113*(46), 13,098–13,103, doi:10.1073/pnas.1604088113.

Bohrer, G., H. Mourad, T. A. Laursen, D. Drewry, R. Avissar, D. Poggi, R. Oren, and G. G. Katul (2005), Finite element tree crown hydrodynamics model (fetch) using porous media flow within branching elements: A new representation of tree hydrodynamics, *Water Resources Research*, *41*(11), doi:10.1029/2005WR004181.

Bonan, G. B., P. J. Lawrence, K. W. Oleson, S. Levis, M. Jung, M. Reichstein, D. M. Lawrence, and S. C. Swenson (2011), Improving canopy processes in the Community Land Model version 4 (CLM4) using global flux fields empirically inferred from FLUXNET data, *Journal of Geophysical Research*, *116*, doi:10.1029/2010JG001593.

Bonan, G. B., M. Williams, R. A. Fisher, and K. W. Oleson (2014), Modeling stomatal conductance in the earth system: linking leaf water-use efficiency and water transport along the soil-plant-atmosphere continuum, *Geoscientific Model Development*, *7*(5), 2193–2222, doi:10.5194/gmd-7-2193-2014.

Bouda, M., and J. E. Saiers (2017), Dynamic effects of root system architecture improve root water uptake in 1-d process-based soil-root hydrodynamics, *Advances in Water Resources*, *110*, 319 – 334, doi:https://doi.org/10.1016/j.advwatres.2017.10.018.

Boyer, J. S. (1967), Leaf water potentials measured with a pressure chamber, *Plant Physiology*, *42*(1), 133–137, doi:10.1104/pp.42.1.133.

Brooks, J. R., F. C. Meinzer, J. M. Warren, J.-C. Domec, and R. Coulombe (2006), Hydraulic redistribution in a douglas-fir forest: lessons from system manipulations, *Plant, Cell & Environment*, *29*(1), 138–150, doi:10.1111/j.1365-3040.2005.01409.x.

Burgess, S. S. O., M. A. Adams, N. C. Turner, and C. K. Ong (1998), The redistribution of soil water by tree root systems, *Oecologia*, *115*(3), 306–311, doi:10.1007/s004420050521.

Cai, G., J. Vanderborght, M. Langensiepen, A. Schnepf, H. Hüging, and H. Vereecken (2018), Root growth, water uptake, and sap flow of winter wheat in response to different soil water conditions, *Hydrology and Earth System Sciences*, *22*(4), 2449–2470, doi:10.5194/hess-22-2449-2018.

Cai, W., S. Borlace, M. Lengaigne, P. Van Rensch, M. Collins, G. Vecchi, A. Timmermann, A. Santoso, M. J. Mcphaden, L. Wu, M. H. England, G. Wang, E. Guilyardi, and F.-f. Jin (2014), Increasing frequency of extreme El Niño events due to greenhouse warming, *Nature Climate Change*, *4*(2), 111–116.

Celia, M. A., E. T. Bouloutas, and R. L. Zarba (1990), A general mass-conservative numerical solution for the unsaturated flow equation, *Water Resources Research*, *26*(7), 1483–1496, doi:10.1029/WR026i007p01483.

Choat, B., S. Jansen, T. J. Brodribb, H. Cochard, S. Delzon, R. Bhaskar, S. J. Bucci, T. S. Feild, S. M. Gleason, U. G. Hacke, A. L. Jacobsen, F. Lens, H. Maherali, J. MartÃŋnez-Vilalta, S. Mayr, M. Mencuccini, P. J. Mitchell, A. Nardini, J. Pittermann, R. B. Pratt, J. S. Sperry, M. Westoby, I. J. Wright, and A. E. Zanne (2012), Global convergence in the vulnerability of forests to drought, *Nature*, *491*(7426), 752–5.

Christoffersen, B. O., M. Gloor, S. Fauset, N. M. Fyllas, D. R. Galbraith, T. R. Baker, B. Kruijt, L. Rowland, R. A. Fisher, O. J. Binks, S. Sevanto, C. Xu, S. Jansen, B. Choat, M. Mencuccini, N. G. McDowell, and P. Meir (2016), Linking hydraulic traits to tropical forest function in a size-structured and trait-driven model (tfs v.1-hydro), *Geoscientific Model Development*, *9*(11), 4227–4255, doi:10.5194/gmd-9-4227-2016.

Clapp, R. B., and G. M. Hornberger (1978), Empirical equations for some soil hydraulic properties, *Water Resources Research*, *14*(4), 601–604, doi:10.1029/WR014i004p00601.

Collatz, G., J. Ball, C. Grivet, and J. A. Berry (1991), Physiological and environmental regulation of stomatal conductance, photosynthesis and transpiration: a model that includes a laminar boundary layer, *Agricultural and Forest Meteorology*, *54*(2), 107 – 136, doi:http://dx.doi.org/10.1016/0168-1923(91)90002-8.

Couvreur, V., J. Vanderborght, and M. Javaux (2012), A simple three-dimensional macroscopic root water uptake model based on the hydraulic architecture approach, *Hydrology and Earth System Sciences*, *16*(8), 2957–2971, doi:10.5194/hess-16-2957-2012.

da Costa, A. C., D. B. Metcalfe, C. E. Doughty, A. A. de Oliveira, G. F. Neto, M. C. da Costa, J. de Athaydes Silva Junior, L. E. Aragão, S. Almeida, D. R. Galbraith, L. M. Rowland, P. Meir, and Y. Malhi (2014), Ecosystem respiration and net primary productivity after 8-10 years of experimental through-fall reduction in an eastern Amazon forest, *Plant Ecology & Diversity*, *7*(1-2), 7–24, doi:10.1080/17550874.2013.798366.

da Costa, A. C. L., D. Galbraith, S. Almeida, B. Takeshi, T. Portela, M. da Costa, J. ao de Athaydes Silva Junior, A. P. Braga, P. H. L. de Gonçalves, A. A. de Oliveira, R. Fisher, O. L. Phillips, D. B. Metcalfe, P. Levy, and P. Meir (2010), Effect of 7 yr of experimental drought on vegetation dynamics and biomass storage of an eastern amazonian rainforest, *The New Phytologist*, *187*(3), 579–591.

Dai, A. (2013), Increasing drought under global warming in observations and models, *Nature Climate Change*, *3*(1), 52–58.

Dai, Y., R. E. Dickinson, and Y.-P. Wang (2004), A two-big-leaf model for canopy temperature, photosynthesis, and stomatal conductance, *Journal of Climate*, *17*(12), 2281–2299, doi:10.1175/1520-0442(2004)017<2281:ATMFCT>2.0.CO;2.

De Kauwe, M. G., J. Kala, Y.-S. Lin, A. J. Pitman, B. E. Medlyn, R. A. Duursma, G. Abramowitz, Y.-P. Wang, and D. G. Miralles (2015), A test of an optimal stomatal conductance scheme within the CABLE land surface model, *Geoscientific Model Development*, *8*(2), 431–452, doi:10.5194/gmd-8-431-2015.

De Kauwe, M. G., B. E. Medlyn, J. Knauer, and C. A. Williams (2017), Ideas and perspectives: how coupled is the vegetation to the boundary layer?, *Biogeosciences*, *14*(19), 4435–4453, doi:10.5194/bg-14-4435-2017.

Domec, J.-C., J. S. King, A. Noormets, E. Treasure, M. J. Gavazzi, G. Sun, and S. G. McNulty (2010), Hydraulic redistribution of soil water by roots affects whole-stand evapotranspiration and net ecosystem carbon exchange, *The New Phytologist*, *187*(1), 171–183, doi:10.1111/j.1469-8137.2010.03245.x.

Drake, J., S. Power, R. Duursma, B. Medlyn, M. Aspinwall, B. Choat, D. Creek, D. Eamus, C. Maier, S. Pfautsch, R. Smith, M. Tjoelker, and D. Tissue (2017), Stomatal and non-stomatal limitations of photosynthesis for four tree species under drought: A comparison of model formulations, *Agricultural and Forest Meteorology*, *247*, 454 – 466, doi:https://doi.org/10.1016/j.agrformet.2017.08.026.

Egea, G., A. Verhoef, and P. L. Vidale (2011), Towards an improved and more flexible representation of water stress in coupled photosynthesis-stomatal conductance models, *Agricultural and Forest Meteorology*, *151*(10), 1370 – 1384, doi:https://doi.org/10.1016/j.agrformet.2011.05.019.

Entekhabi, D., E. G. Njoku, P. E. O'Neill, K. H. Kellogg, W. T. Crow, W. N. Edelstein, J. K. Entin, S. D. Goodman, T. J. Jackson, J. Johnson, J. Kimball, J. R. Piepmeier, R. D. Koster, N. Martin, K. C. McDonald, M. Moghaddam, S. Moran, R. Reichle, J. C. Shi, M. W. Spencer, S. W. Thurman, L. Tsang, and J. V. Zyl (2010), The soil moisture active passive (smap) mission, *Proceedings of the IEEE*, *98*(5), 704–716, doi: 10.1109/JPROC.2010.2043918.

Epila, J., N. J. De Baerdemaeker, L. L. Vergeynst, W. H. Maes, H. Beeckman, and K. Steppe (2017), Capacitive water release and internal leaf water relocation delay drought-induced cavitation in African Maesopsis eminii, *Tree Physiology*, *37*(4), 481–490, doi: 10.1093/treephys/tpw128.

Farquhar, G. D., S. von Caemmerer, and J. A. Berry (1980), A biochemical model of photosynthetic CO_2 assimilation in leaves of C_3 species, *Planta*, *149*(1), 78–90, doi: 10.1007/BF00386231.

Ficklin, D. L., and K. A. Novick (2017), Historic and projected changes in vapor pressure deficit suggest a continentalâĂŘscale drying of the United States atmosphere, *Journal of Geophysical Research: Atmospheres*, *122*(4), 2061–2079, doi:10.1002/2016JD025855.

Fisher, R. A., M. Williams, R. L. Do Vale, A. L. Da Costa, and P. Meir (2006), Evidence from Amazonian forests is consistent with isohydric control of leaf water potential, *Plant, Cell & Environment*, *29*(2), 151–165, doi:10.1111/j.1365-3040.2005.01407.x.

Fisher, R. A., M. Williams, A. L. D. Costa, Y. Malhi, R. F. D. Costa, S. Almeida, and P. Meir (2007), The response of an Eastern Amazonian rain forest to drought stress: results and modelling analyses from a throughfall exclusion experiment, *Global Change Biology*, *13*(11), 2361–2378, doi:10.1111/j.1365-2486.2007.01417.x.

Fisher, R. A., M. Williams, M. de Lourdes Ruivo, A. L. de Costa, and P. Meir (2008), Evaluating climatic and soil water controls on evapotranspiration at two Amazonian rainforest sites, *Agricultural and Forest Meteorology*, *148*(6), 850 – 861, doi: https://doi.org/10.1016/j.agrformet.2007.12.001.

Flexas, J., J. Bota, F. Loreto, G. Cornic, and T. D. Sharkey (2004), Diffusive and metabolic limitations to photosynthesis under drought and salinity in c3 plants, *Plant Biology*, *6*(3), 269–279, doi:10.1055/s-2004-820867.

Flexas, J., M. Ribas-Carbó, J. Bota, J. Galmés, M. Henkle, S. Martínez-Cañellas, and H. Medrano (2006), Decreased rubisco activity during water stress is not induced by decreased relative water content but related to conditions of low stomatal conductance and chloroplast CO2 concentration, *New Phytologist*, *172*(1), 73–82, doi:10.1111/j.1469-8137.2006.01794.x.

Franks, P. J., P. L. Drake, and R. H. Froend (2007), Anisohydric but isohydrodynamic: seasonally constant plant water potential gradient explained by a stomatal control mechanism incorporating variable plant hydraulic conductance, *Plant, Cell & Environment*, *30*(1), 19–30, doi:10.1111/j.1365-3040.2006.01600.x.

Friedlingstein, P., M. Meinshausen, V. K. Arora, C. D. Jones, A. Anav, S. K. Liddicoat, and R. Knutti (2014), Uncertainties in CMIP5 climate projections due to carbon cycle feedbacks, *Journal of Climate*, *27*(2), 511–526.

Fu, R., L. Yin, W. Li, P. A. Arias, R. E. Dickinson, L. Huang, S. Chakraborty, K. Fernandes, B. Liebmann, R. Fisher, and R. B. Myneni (2013), Increased dry-season length over southern Amazonia in recent decades and its implication for future climate projection, *Proceedings of the National Academy of Sciences of the United States of America*, *110*(45), 18,110–18,115.

Gentine, P., M. Guérin, M. Uriarte, N. G. McDowell, and W. T. Pockman (2016), An allometry-based model of the survival strategies of hydraulic failure and carbon starvation, *Ecohydrology*, *9*(3), 529–546, doi:10.1002/eco.1654.

Grant, J., J.-P. Wigneron, R. D. Jeu, H. Lawrence, A. Mialon, P. Richaume, A. A. Bitar, M. Drusch, M. van Marle, and Y. Kerr (2016), Comparison of SMOS and AMSR-E vegetation optical depth to four MODIS-based vegetation indices, *Remote Sensing of Environment*, *172*, 87 – 100, doi:https://doi.org/10.1016/j.rse.2015.10.021.

Green, J. K., A. G. Konings, S. H. Alemohammad, J. Berry, D. Entekhabi, J. Kolassa, J.-E. Lee, and P. Gentine (2017), Regionally strong feedbacks between the atmosphere and terrestrial biosphere, *Nature Geoscience*, *10*(6), 410–414, doi:10.1038/ngeo2957.

Harley, P. C., R. B. Thomas, J. F. Reynolds, and B. R. Strain (1992), Modelling photosynthesis of cotton grown in elevated co2, *Plant Cell Environment*, *15*(3), 271–282, doi:10.1111/j.1365-3040.1992.tb00974.x.

Holbrook, N. M., E. T. Ahrens, M. J. Burns, and M. A. Zwieniecki (2001), In vivo observation of cavitation and embolism repair using magnetic resonance imaging, *Plant Physiology*, *126*(1), 27–31, doi:10.1104/pp.126.1.27.

Jackson, R. B., J. Canadell, J. R. Ehleringer, H. A. Mooney, O. E. Sala, and E. D. Schulze (1996), A global analysis of root distributions for terrestrial biomes, *Oecologia*, *108*(3), 389–411, doi:10.1007/BF00333714.

Jackson, R. B., J. S. Sperry, and T. E. Dawson (2000), Root water uptake and transport: using physiological processes in global predictions, *Trends in Plant Science*, *5*(11), 482 – 488, doi:https://doi.org/10.1016/S1360-1385(00)01766-0.

Joetzjer, E., C. Delire, H. Douville, P. Ciais, B. Decharme, R. Fisher, B. Christoffersen, J. C. Calvet, A. C. L. da Costa, L. V. Ferreira, and P. Meir (2014), Predicting the response of the Amazon rainforest to persistent drought conditions under current and future climates: a major challenge for global land surface models, *Geoscientific Model Development*, *7*(6), 2933–2950, doi:10.5194/gmd-7-2933-2014.

Kattge, J., S. DÃŊAz, S. Lavorel, I. C. Prentice, P. Leadley, G. BÃŰNisch, E. Garnier, M. Westoby, P. B. Reich, I. J. Wright, J. H. C. Cornelissen, C. Violle, S. P. Harrison, P. M. Van Bodegom, M. ReichSTEIN, B. J. Enquist, N. A. Soudzilovskaia, D. D. Ackerly, M. Anand, O. Atkin, M. Bahn, T. R. Baker, D. Baldocchi, R. Bekker, C. C. Blanco, B. Blonder, W. J. Bond, R. Bradstock, D. E. Bunker, F. Casanoves, J. Cavender-Bares, J. Q. Chambers, F. S. Chapin Iii, J. Chave, D. Coomes, W. K. Cornwell, J. M. Craine, B. H. Dobrin, L. Duarte, W. Durka, J. Elser, G. Esser, M. Estiarte, W. F. Fagan, J. Fang, F. FernÃĄNdez-MÃĽNdez, A. Fidelis, B. Finegan, O. Flores, H. Ford, D. Frank, G. T. Freschet, N. M. Fyllas, R. V. Gallagher, W. A. Green, A. G. Gutierrez, T. Hickler, S. I. Higgins, J. G. Hodgson, A. Jalili, S. Jansen, C. A. Joly, A. J. Kerkhoff, D. Kirkup, K. Kitajima, M. Kleyer, S. Klotz, J. M. H. Knops, K. Kramer, I. KÃIJHn, H. Kurokawa, D. Laughlin, T. D. Lee, M. Leishman, F. Lens, T. Lenz, S. L. Lewis, J. Lloyd, J. LlusiÃĂ, F. Louault, S. Ma, M. D. MaHECHA, P. MaNNING, T. MaSSAD, B. E. Medlyn, J. Messier, A. T. Moles, S. C. MÃIJLler, K. Nadrowski, S. Naeem, Ã. Niinemets, S. NÃŰLlerT, A. NÃIJSke, R. Ogaya, J. Oleksyn, V. G. Onipchenko, Y. Onoda, J. OrdoÃŚEz, G. Overbeck, W. A. Ozinga, S. PatiÃŚO, S. Paula, J. G. Pausas, J. PeÃŚUelas, O. L. Phillips, V. Pillar, H. Poorter, L. Poorter, P. Poschlod, A. Prinzing, R. Proulx, A. Rammig, S. Reinsch, B. Reu, L. Sack, B. Salgado-Negret, J. Sardans, S. Shiodera, B. Shipley, A. Siefert, E. Sosinski, J.-F. Soussana, E. Swaine, N. Swenson, K. Thompson, P. Thornton, M. Waldram, E. Weiher, M. White, S. White, S. J. Wright, B. Yguel, S. Zaehle, A. E. Zanne, and C. Wirth (2011), Try âĂŞ a global database of plant traits, *Global Change Biology*, *17*(9), 2905–2935, doi:10.1111/j.1365-2486.2011.02451.x.

Klein, T., and S. Niu (2014), The variability of stomatal sensitivity to leaf water potential across tree species indicates a continuum between isohydric and anisohydric behaviours, *Functional Ecology*, *28*(6), 1313–1320, doi:10.1111/1365-2435.12289.

Konings, A. G., and P. Gentine (2017a), Global variations in ecosystem-scale isohydricity, *Global Change Biology*, *23*(2), 891–905, doi:10.1111/gcb.13389.

Konings, A. G., M. Piles, K. RÃűtzer, K. A. McColl, S. K. Chan, and D. Entekhabi (2016), Vegetation optical depth and scattering albedo retrieval using time series of dual-polarized l-band radiometer observations, *Remote Sensing of Environment*, *172*, 178 – 189, doi:https://doi.org/10.1016/j.rse.2015.11.009.

Konings, A. G., A. P. Williams, and P. Gentine (2017b), Sensitivity of grassland productivity to aridity controlled by stomatal and xylem regulation, *Nature Geoscience*, *10*(4), 284–288, doi:10.1038/ngeo2903.

Kotowska, M. M., D. Hertel, Y. A. Rajab, H. Barus, and B. Schuldt (2015), Patterns in hydraulic architecture from roots to branches in six tropical tree species from cacao agroforestry and their relation to wood density and stem growth, *Frontiers in Plant Science*, *6*, 191, doi:10.3389/fpls.2015.00191.

Lee, J.-E., R. S. Oliveira, T. E. Dawson, and I. Fung (2005), Root functioning modifies seasonal climate, *Proceedings of the National Academy of Sciences of the United States of America*, *102*(49), 17,576–17,581, doi:10.1073/pnas.0508785102.

Lin, C., P. Gentine, Y. Huang, K. Guan, H. Kimm, and S. Zhou (2018), Diel ecosystem conductance response to vapor pressure deficit is suboptimal and independent of soil moisture, *Agricultural and Forest Meteorology*, *250-251*, 24 – 34, doi: https://doi.org/10.1016/j.agrformet.2017.12.078.

Mackay, D. S., D. E. Roberts, B. E. Ewers, J. S. Sperry, N. G. McDowell, and W. T. Pockman (2015), Interdependence of chronic hydraulic dysfunction and canopy processes can improve integrated models of tree response to drought, *Water Resources Research*, *51*(8), 6156–6176, doi:10.1002/2015WR017244.

Manzoni, S., G. Vico, G. Katul, P. A. Fay, W. Polley, S. Palmroth, and A. Porporato (2011), Optimizing stomatal conductance for maximum carbon gain under water stress: a meta-analysis across plant functional types and climates, *Functional Ecology*, *25*(3), 456–467, doi:10.1111/j.1365-2435.2010.01822.x.

Manzoni, S., G. Vico, S. Palmroth, A. Porporato, and G. Katul (2013a), Optimization of stomatal conductance for maximum carbon gain under dynamic soil moisture, *Advances in Water Resources*, *62*, 90 – 105, doi:https://doi.org/10.1016/j.advwatres.2013.09.020.

Manzoni, S., G. Vico, G. Katul, S. Palmroth, R. B. Jackson, and A. Porporato (2013b), Hydraulic limits on maximum plant transpiration and the emergence of the safety-efficiency trade-off, *New Phytologist*, *198*(1), 169–178, doi:10.1111/nph.12126.

McDowell, N., C. D. Allen, â. K. Anderson, P. Brando, R. Brienen, J. Chambers, B. Christoffersen, S. Davies, C. Doughty, A. Duque, F. EspiritoâĂŘSanto, R. Fisher, C. G. Fontes, D. Galbraith, D. Goodsman, C. Grossiord, H. Hartmann, J. Holm, D. J. Johnson, A. R. Kassim, M. Keller, C. Koven, L. Kueppers, T. Kumagai, Y. Malhi, S. M. McMahon, M. Mencuccini, P. Meir, P. Moorcroft, â. H. C. Muller, O. L. Phillips, T. Powell, C. A. Sierra, J. Sperry, J. Warren, C. Xu, and X. Xu (2018), Drivers and mechanisms of tree mortality in moist tropical forests, *New Phytologist*, *0*(0), doi:10.1111/nph.15027.

Mcdowell, N. G., and C. D. Allen (2015), Darcy's law predicts widespread forest mortality under climate warming, *Nature Climate Change*, *5*(7), 669–672.

McDowell, N. G., R. A. Fisher, C. Xu, J. C. Domec, T. HÃűlttÃď, D. S. Mackay, J. S. Sperry, A. Boutz, L. Dickman, N. Gehres, J. M. Limousin, A. Macalady, J. MartÃŋnez-Vilalta, M. Mencuccini, J. A. Plaut, J. OgÃľe, R. E. Pangle, D. P. Rasse, M. G. Ryan, S. Sevanto, R. H. Waring, A. P. Williams, E. A. Yepez, and W. T. Pockman (2013), Evaluating theories of drought-induced vegetation mortality using a multimodelâĂŞexperiment framework, *New Phytologist*, *200*(2), 304–321, doi:10.1111/nph.12465.

McDowell, N. G., A. P. Williams, C. Xu, W. T. Pockman, L. T. Dickman, S. Sevanto, R. Pangle, J. Limousin, J. Plaut, D. S. Mackay, J. Ogee, J. C. Domec, C. D. Allen, R. A. Fisher, X. Jiang, J. D. Muss, D. D. Breshears, S. A. Rauscher, and C. Koven (2016), Multi-scale predictions of massive conifer mortality due to chronic temperature rise, *Nature Climate Change*, *6*, 295–300, doi:10.1038/nclimate2873.

Medlyn, B. E., R. A. Duursma, D. Eamus, D. S. Ellsworth, I. C. Prentice, C. V. M. Barton, K. Y. Crous, P. De Angelis, M. Freeman, and L. Wingate (2011), Reconciling the optimal and empirical approaches to modelling stomatal conductance, *Global Change Biology*, *17*(6), 2134–2144, doi:10.1111/j.1365-2486.2010.02375.x.

Meinzer, F. C., S. A. James, and G. Goldstein (2004), Dynamics of transpiration, sap flow and use of stored water in tropical forest canopy trees, *Tree Physiology*, *24*(8), 901–909, doi:10.1093/treephys/24.8.901.

Meinzer, F. C., D. M. Johnson, B. Lachenbruch, K. A. McCulloh, and D. R. Woodruff (2009), Xylem hydraulic safety margins in woody plants: coordination of stomatal con-

trol of xylem tension with hydraulic capacitance, *Functional Ecology*, *23*(5), 922–930, doi:10.1111/j.1365-2435.2009.01577.x.

Momen, M., J. D. Wood, K. A. Novick, R. Pangle, W. T. Pockman, N. G. McDowell, and A. G. Konings (2017), Interacting effects of leaf water potential and biomass on vegetation optical depth, *Journal of Geophysical Research: Biogeosciences*, *122*(11), 3031–3046, doi:10.1002/2017JG004145.

Nepstad, D. C., R. de Carvalho, Claudio, E. A. Davidson, P. H. Jipp, and e. al (1994), The role of deep roots in the hydrological and carbon cycles of amazonian forests and pastures, *Nature*, *372*(6507), 666.

Novick, K. A., D. L. Ficklin, P. C. Stoy, C. A. Williams, G. Bohrer, A. Oishi, S. A. Papuga, P. D. Blanken, A. Noormets, B. N. Sulman, R. L. Scott, L. Wang, and R. P. Phillips (2016a), The increasing importance of atmospheric demand for ecosystem water and carbon fluxes, *Nature Climate Change*, *6*(11), 1023–1027.

Novick, K. A., C. F. Miniat, and J. M. Vose (2016b), Drought limitations to leaf-level gas exchange: results from a model linking stomatal optimization and cohesion-tension theory, *Plant, Cell & Environment*, *39*(3), 583–596, doi:10.1111/pce.12657.

Oleson, K. W., D. M. Lawrence, G. B. Bonan, B. Drewniak, M. Huang, C. D. Koven, S. Levis, F. Li, W. J. Riley, Z. M. Subin, S. C. Swenson, P. E. Thornton, A. Bozbiyik, R. Fisher, C. L. Heald, E. Kluzek, J.-F. Lamarque, P. J. Lawrence, L. R. Leung, W. Lipscomb, S. Muszala, D. M. Ricciuto, W. Sacks, Y. Sun, J. Tang, and Z.-L. Yang (2013), Technical description of version 4.5 of the community land model (clm), NCAR Tech. Note NCAR/TN-503+STR, *National Center for Atmospheric Research, Boulder, Colorado, 420 pp.*, doi:10.5065/D6RR1W7M.

Oliveira, R. S., T. E. Dawson, S. S. O. Burgess, and D. C. Nepstad (2005), Hydraulic redistribution in three amazonian trees, *Oecologia*, *145*(3), 354–363, doi:10.1007/s00442-005-0108-2.

Powell, T. L., D. R. Galbraith, B. O. Christoffersen, A. Harper, H. M. A. Imbuzeiro, L. Rowland, S. Almeida, P. M. Brando, A. C. L. da Costa, M. H. Costa, N. M. Levine, Y. Malhi, S. R. Saleska, E. Sotta, M. Williams, P. Meir, and P. R. Moorcroft (2013), Confronting model predictions of carbon fluxes with measurements of amazon forests subjected to experimental drought, *New Phytologist*, *200*(2), 350–365, doi:10.1111/nph.12390.

Powell, T. L., W. J. K., O. A. A. R., C. A. C. Lola, S. S. R., M. Patrick, and M. P. R. (2018), Differences in xylem and leaf hydraulic traits explain differences in drought tolerance among mature amazon rainforest trees, *Global Change Biology*, *23*(10), 4280–4293, doi:10.1111/gcb.13731.

Restaino, C. M., D. L. Peterson, and J. Littell (2016), Increased water deficit decreases douglas fir growth throughout western US forests, *Proceedings of the National Academy of Sciences*, *113*(34), 9557–9562, doi:10.1073/pnas.1602384113.

Restrepo-Coupe, N., N. M. Levine, B. O. Christoffersen, L. P. Albert, J. Wu, M. H. Costa, D. Galbraith, H. Imbuzeiro, G. Martins, A. C. da Araujo, Y. S. Malhi, X. Zeng, P. Moorcroft, and S. R. Saleska (2017), Do dynamic global vegetation models capture the seasonality of carbon fluxes in the amazon basin? A data-model intercomparison, *Global Change Biology*, *23*(1), 191–208, doi:10.1111/gcb.13442.

Rogers, A., B. E. Medlyn, J. S. Dukes, G. Bonan, S. Caemmerer, M. C. Dietze, J. Kattge, A. D. B. Leakey, L. M. Mercado, Ã. Niinemets, I. C. Prentice, S. P. Serbin, S. Sitch, D. A. Way, and S. Zaehle (2017), A roadmap for improving the representation of photosynthesis in earth system models, *New Phytologist*, *213*(1), 22–42, doi:10.1111/nph.14283.

Sack, L., P. J. Melcher, M. A. Zwieniecki, and N. M. Holbrook (2002), The hydraulic conductance of the angiosperm leaf lamina: a comparison of three measurement methods, *Journal of Experimental Botany*, *53*(378), 2177–2184.

Scholz, F. G., N. G. Phillips, S. J. Bucci, F. C. Meinzer, and G. Goldstein (2011), Hydraulic capacitance: Biophysics and functional significance of internal water sources, in Meinzer, F.C., Lachenbruch, B., Dawson, T. E. (eds) *Size- and Age-Related Changes in Tree Structure and Function*, pp. 341–361, Springer, Dordrecht.

Seager, R., A. Hooks, A. P. Williams, B. Cook, J. Nakamura, and N. Henderson (2015), Climatology, variability, and trends in the u.s. vapor pressure deficit, an important fire-related meteorological quantity, *Journal of Applied Meteorology and Climatology*, *54*(6), 1121–1141, doi:10.1175/JAMC-D-14-0321.1.

Sellers, P. J., D. A. Randall, G. J. Collatz, J. A. Berry, C. B. Field, D. A. Dazlich, C. Zhang, G. D. Collelo, and L. Bounoua (1996a), a revised land surface parameterization (sib2) for atmospheric gcms. part i: Model formulation, *Journal of Climate*, *9*(4), 676–705, doi:10.1175/1520-0442(1996)009<0676:ARLSPF>2.0.CO;2.

Sellers, P. J., C. J. Tucker, G. J. Collatz, S. O. Los, C. O. Justice, D. A. Dazlich, and D. A. Randall (1996b), A revised land surface parameterization (sib2) for atmospheric gcms. part ii: The generation of global fields of terrestrial biophysical parameters from satellite data, *Journal of Climate*, *9*(4), 706–737, doi:10.1175/1520-0442(1996)009<0706:ARLSPF>2.0.CO;2.

Sheffield, J., E. F. Wood, and M. L. Roderick (2012), Little change in global drought over the past 60 years, *Nature*, *491*(7424), 435–8.

Simonin, K. A., E. Burns, B. Choat, M. M. Barbour, T. E. Dawson, and P. J. Franks (2015), Increasing leaf hydraulic conductance with transpiration rate minimizes the water potential drawdown from stem to leaf, *Journal of Experimental Botany*, *66*(5), 1303–1315, doi:10.1093/jxb/eru481.

Siqueira, M., G. Katul, and A. Porporato (2008), Onset of water stress, hysteresis in plant conductance, and hydraulic lift: Scaling soil water dynamics from millimeters to meters, *Water Resources Research*, *44*(1), W01,432, doi:10.1029/2007WR006094.

Sperry, J. S., and D. M. Love (2015), What plant hydraulics can tell us about responses to climate-change droughts, *New Phytologist*, *207*(1), 14–27, doi:10.1111/nph.13354.

Sperry, J. S., F. R. Adler, G. S. Campbell, and J. P. Comstock (1998), Limitation of plant water use by rhizosphere and xylem conductance: results from a model, *Plant Cell Environment*, *21*(4), 347–359, doi:10.1046/j.1365-3040.1998.00287.x.

Sperry, J. S., U. G. Hacke, R. Oren, and J. P. Comstock (2002), Water deficits and hydraulic limits to leaf water supply, *Plant, Cell & Environment*, *25*(2), 251–263, doi:10.1046/j.0016-8025.2001.00799.x.

Sperry, J. S., M. D. Venturas, W. R. L. Anderegg, M. Mencuccini, D. S. Mackay, Y. Wang, and D. M. Love (2017), Predicting stomatal responses to the environment from the optimization of photosynthetic gain and hydraulic cost, *Plant, Cell & Environment*, *40*(6), 816–830, doi:10.1111/pce.12852, pCE-16-0541.R1.

Thornton, P. E., and N. E. Zimmermann (2007), An improved canopy integration scheme for a land surface model with prognostic canopy structure, *Journal of Climate*, *20*(15), 3902–3923, doi:10.1175/JCLI4222.1.

Tyree, M. T., and J. S. Sperry (1988), Do woody plants operate near the point of catastrophic xylem dysfunction caused by dynamic water stress?: Answers from a model, *Plant Physiology*, *88*(3), 574–580.

Tyree, M. T., and J. S. Sperry (1989), Vulnerability of xylem to cavitation and embolism, *Annual Review of Plant Physiology and Plant Molecular Biology*, *40*(1), 19–36, doi:10.1146/annurev.pp.40.060189.000315.

Ukkola, A. M., M. G. D. Kauwe, A. J. Pitman, M. J. Best, G. Abramowitz, V. Haverd, M. Decker, and N. Haughton (2016), Land surface models systematically overestimate the intensity, duration and magnitude of seasonal-scale evaporative droughts, *Environmental Research Letters*, *11*(10), 104,012.

Verhoef, A., and G. Egea (2014), Modeling plant transpiration under limited soil water: Comparison of different plant and soil hydraulic parameterizations and preliminary implications for their use in land surface models, *Agricultural and Forest Meteorology*, *191*, 22–32, doi:https://doi.org/10.1016/j.agrformet.2014.02.009.

Warren, J. M., P. J. Hanson, C. M. Iversen, J. Kumar, A. P. Walker, and S. D. Wullschleger (), Root structural and functional dynamics in terrestrial biosphere models âĂŞ evaluation and recommendations, *New Phytologist*, *205*(1), 59–78, doi:10.1111/nph.13034.

Williams, A. P., C. D. Allen, A. K. Macalady, D. Griffin, C. A. Woodhouse, D. M. Meko, T. W. Swetnam, S. A. Rauscher, R. Seager, H. Grissino-Mayer, J. S. Dean, E. R. Cook, C. Gangodagamage, M. Cai, and N. G. Mcdowell (2013), Temperature as a potent driver of regional forest drought stress and tree mortality, *Nature Climate Change*, *3*(3), 292–297.

Williams, M., E. B. Rastetter, D. N. Fernandes, M. L. Goulden, S. C. Wofsy, G. R. Shaver, J. M. Melillo, J. W. Munger, S.-M. Fan, and K. J. Nadelhoffer (1996), Modelling the soil-plant-atmosphere continuum in a quercusâĂŞacer stand at harvard forest: the regulation of stomatal conductance by light, nitrogen and soil/plant hydraulic properties, *Plant, Cell & Environment*, *19*(8), 911–927, doi:10.1111/j.1365-3040.1996.tb00456.x.

Williams, M., B. E. Law, P. M. Anthoni, and M. H. Unsworth (2001), Use of a simulation model and ecosystem flux data to examine carbonâĂŞwater interactions in ponderosa pine., *Tree Physiology*, *21*(5), 287 – 298.

Xu, X., D. Medvigy, J. S. Powers, J. M. Becknell, and K. Guan (2016), Diversity in plant hydraulic traits explains seasonal and inter-annual variations of vegetation dynamics in seasonally dry tropical forests, *New Phytologist*, *212*(1), 80–95, doi:10.1111/nph.14009, 2015-20772.

Zhou, S., R. A. Duursma, B. E. Medlyn, J. W. Kelly, and I. C. Prentice (2013), How should we model plant responses to drought? An analysis of stomatal and non-stomatal responses to water stress, *Agricultural and Forest Meteorology*, *182-183*, 204 – 214, doi: https://doi.org/10.1016/j.agrformet.2013.05.009.

Zhou, S., B. Medlyn, S. Sabaté, D. Sperlich, I. C. Prentice, and D. Whitehead (2014), Short-term water stress impacts on stomatal, mesophyll and biochemical limitations to photosynthesis differ consistently among tree species from contrasting climates, *Tree Physiology*, *34*(10), 1035, doi:10.1093/treephys/tpu072.